THE GEOLOGICAL SOCIETY OF AMERICA®

Late Mesozoic–Cenozoic cooling history of the northeastern Tibetan Plateau and its foreland derived from low-temperature thermochronology

Chen Wu[1,†], Andrew V. Zuza[2], Jie Li[3], Peter J. Haproff[4], An Yin[5], Xuanhua Chen[6], Lin Ding[1,7], and Bing Li[2,6]

[1]*Key Laboratory of Continental Collision and Plateau Uplift, Institute of Tibetan Plateau Research, and Center for Excellence in Tibetan Plateau Earth Sciences, Chinese Academy of Sciences, Beijing 100101, China*

[2]*Nevada Bureau of Mines and Geology, University of Nevada, Reno, Nevada 89557, USA*

[3]*School of Earth Sciences and Resources, China University of Geosciences, Beijing 100083 China*

[4]*Department of Earth and Ocean Sciences, University of North Carolina, Wilmington, North Carolina 28403, USA*

[5]*Department of Earth, Planetary and Space Sciences, University of California, Los Angeles, California 90095, USA*

[6]*Chinese Academy of Geological Sciences, Beijing 100037, China*

[7]*University of Chinese Academy of Sciences, Beijing 100049, China*

ABSTRACT

The growth history and formation mechanisms of the Cenozoic Tibetan Plateau are the subject of an intense debate with important implications for understanding the kinematics and dynamics of large-scale intracontinental deformation. Better constraints on the uplift and deformation history across the northern plateau are necessary to address how the Tibetan Plateau was constructed. To this end, we present updated field observations coupled with low-temperature thermochronology from the Qaidam basin in the south to the Qilian Shan foreland in the north. Our results show that the region experienced a late Mesozoic cooling event that is interpreted as a result of tectonic deformation prior to the India-Asia collision. Our results also reveal the onset of renewed cooling in the Eocene in the Qilian Shan region along the northern margin of the Tibetan Plateau, which we interpret to indicate the timing of initial thrusting and plateau formation along the plateau margin. The interpreted Eocene thrusting in the Qilian Shan predates Cenozoic thrust belts to the south (e.g., the Eastern Kunlun Range), which supports out-of-sequence rather than northward-migrating thrust belt development. The early Cenozoic deformation exploited the south-dipping early Paleozoic Qilian suture zone as indicated by our field mapping and the existing geophysical data. In the Miocene, strike-slip faulting was initiated along segments of the older Paleozoic suture zones in northern Tibet, which led to the development of the Kunlun and Haiyuan left-slip transpressional systems. Late Miocene deformation and uplift of the Hexi corridor and Longshou Shan directly north of the Qilian Shan thrust belt represent the most recent phase of outward plateau growth.

INTRODUCTION

Although establishing the evolution of the Cenozoic India-Asia collision zone has profound implications for deciphering the intracontinental-deformation mechanisms (i.e., England and Houseman, 1986; Burchfiel and Royden, 1991; Yin and Harrison, 2000; Royden et al., 2008; Taylor and Yin 2009; Clark et al., 2010; Yin, 2010; Ren et al., 2013; Clark, 2012; Fan and Murphy, 2021) (Fig. 1), the spatiotemporal evolution of the Tibetan Plateau remains a subject of debate (e.g., Tapponnier et al., 2001; Yin et al., 2008a, 2008b; Wang et al., 2020a). This debate has inspired research activities in northern Tibet in the past decades between the Eastern Kunlun in the south and the Qilian Shan in the north (e.g., Meyer et al., 1998; Yuan et al., 2013; Duvall et al., 2011; Clark, 2012; Zheng et al., 2017; Zuza et al., 2016, 2019; Li et al., 2019, 2020; Yu et al., 2019a, 2019b; An et al., 2020) (Fig. 2A), which has centered on testing two end-member tectonic models: (1) the compressional deformation front migrated progressively on in a stepwise jump northward from the Himalayan collisional front in the south to the northern plateau margin (e.g., England and Houseman, 1986; Burchfiel and Royden, 1991; Tapponnier et al., 2001; Wang et al., 2014; Yu et al., 2019a, 2019b; Zheng et al., 2017; Wang et al., 2020a) or (2) early phase India-Asia collision caused compressional deformation along the northern and southern margins of the plateau, and the deformation zones progressively migrated inward to the plateau interior (e.g., Yin and Harrison, 2000; Clark, 2012; Staisch et al., 2016; Zuza et al., 2019, 2020; Li et al., 2019, 2020; Chen et al., 2019a, 2019b; Cheng et al., 2019; Wu et al., 2019a; Bian et al., 2020; Chen et al., 2020). The two end-member models make specific predictions about the timing and style of deformation that can be tested by combined field observations and thermochronological studies (Fig. 2A).

In this study we integrated systematic geologic mapping, field observations, and apatite fission-track (AFT) thermochronology across key regions in the Qilian Shan and its foreland region to document the deformation-related exhumation history of the northeastern margin of the Tibetan Plateau and region to the northeast (Fig. 2B; Table S1[1]). We focused on AFT analysis and thermal history modeling of 29 pre-Cenozoic granitoid and sedimentary bedrock samples collected in fault-bounded ranges to elucidate the cooling history of this region since the late Mesozoic and shed light on the basin range evolution across the northeastern plateau that has since experienced multiple phases of growth. We

[†]wuchen@itpcas.ac.cn; wuchenlovegeology@gmail.com.

[1]Supplemental Material. The original field pictures and summary of thermochronology data in north Tibet. Please visit https://doi.org/10.1130/GSAB.S.13718050 to access the supplemental material, and contact editing@geosociety.org with any questions.

 https://doi.org/10.1130/B35879.1; 11 figures; 2 tables; 1 supplemental file.

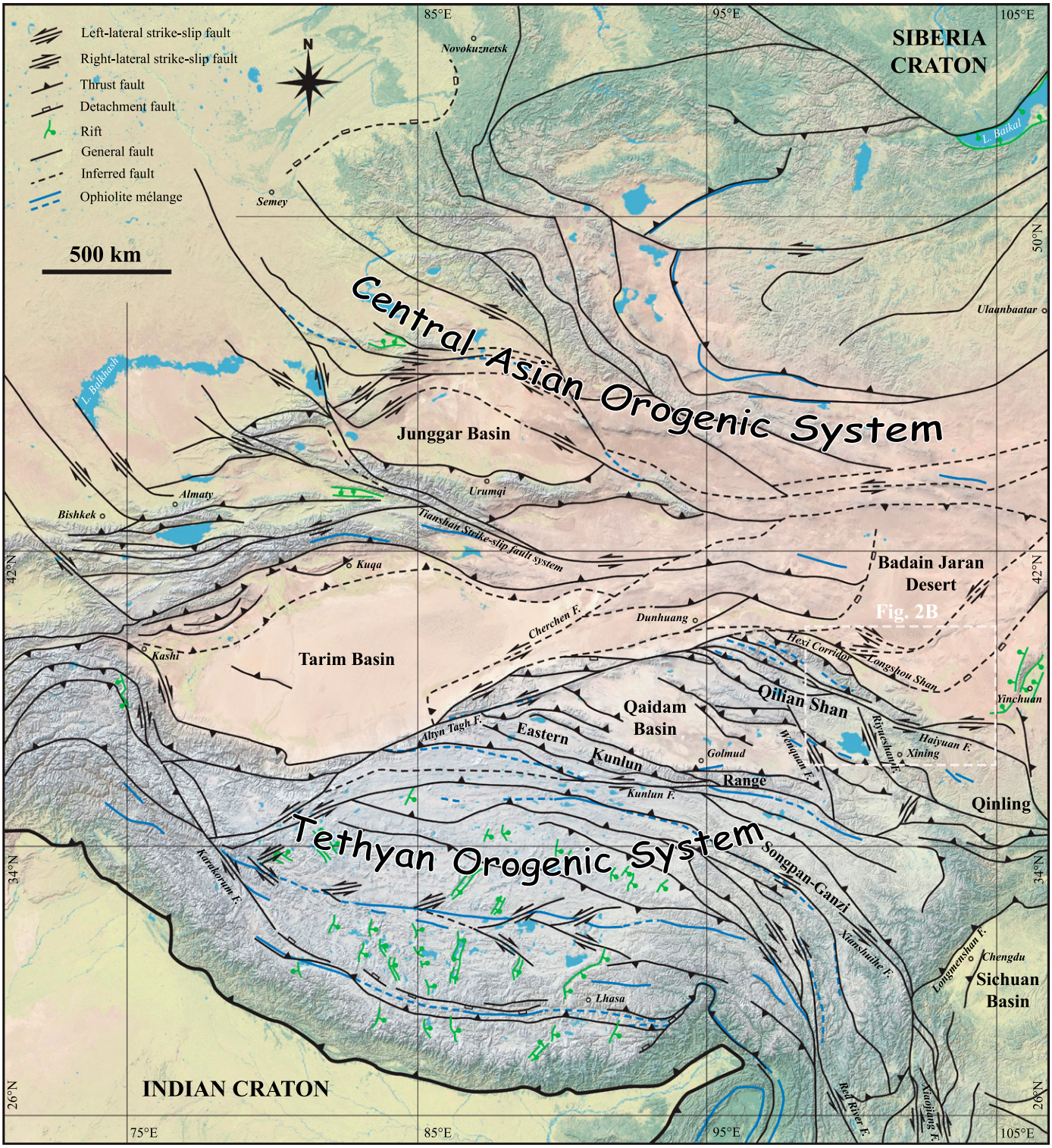

Figure 1. Fault map shows the central Asian orogenic system and the Tethyan orogenic system. Sources of information are from Ren et al. (2013), Taylor et al. (2003), and Yin (2010). The white dashed box shows the location of Figure 2B.

further develop a deformation history model of the Qilian Shan thrusts with detailed field observations and AFT results from the Cretaceous samples.

GEOLOGICAL SETTING

The northeastern Tibetan Plateau has an average elevation of ~4.5 km, and this high topography decreases rapidly to <1.5 km in the Hexi Corridor foreland basin to the north (Figs. 1 and 2A). The northern boundary of the plateau is the Qilian Shan thrust belt and

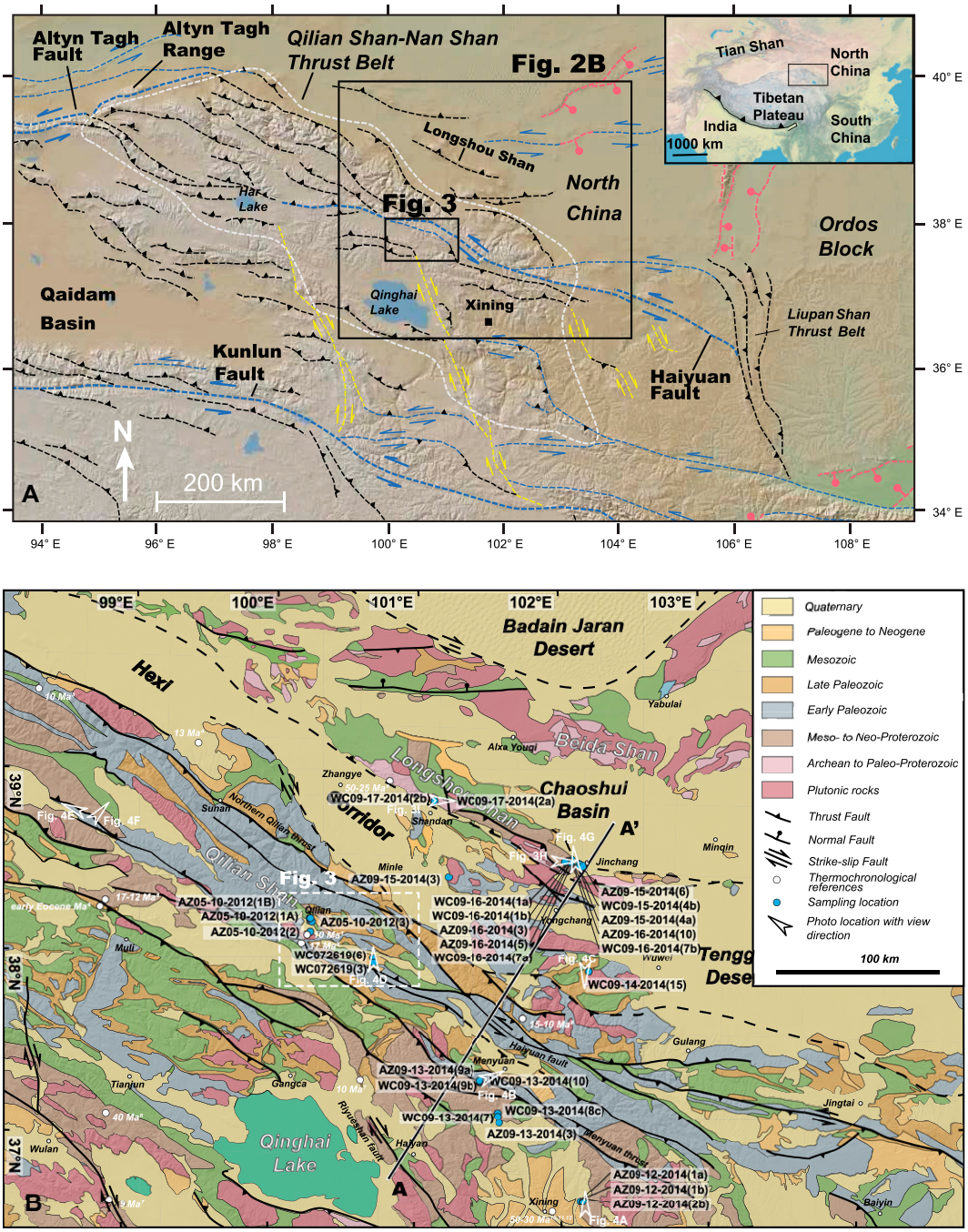

Figure 2. (A) Regional tectonic map shows the northern Tibetan Plateau and its adjacent regions (modified from Gao et al., 2013; Zuza et al., 2016; and Wu et al., 2017). Major faults are denoted with black lines (thrust), blue lines (sinistral strike slip), yellow lines (dextral strike slip), and pink lines (normal). Underlying base map is from www.geomapapp.org (accessed January 2021; Ryan et al., 2009). (B) Simplified geologic map of the northeastern Tibetan Plateau and its northern foreland and cross section of A–A′. Location is shown in Figure 1. The geology was compiled from Gansu Geological Bureau (1969), Qinghai BGMR (1991), Pan et al. (2004), Gong et al. (2013), and our own geologic mapping. The thermochronology data are shown in Table S1 (see footnote 1) with data from: 1—C.C. Liu et al. (2016); 2—J. Pang et al. (2019); 3—D. Zheng et al. (2010); 4—X. Fang et al. (2013); 5—Duvall et al. (2013); 6—B. Qi et al. (2016); 7—D. Yuan et al. (2011); 8—B. Li et al. (2019); 9—B.H. Zhang et al. (2017); 10—Dupont-Nivet et al. (2004); 11—S. Dai et al. (2006); and 12—J. Zhang et al. (2015).

left-slip Haiyuan fault (e.g., Burchfiel et al., 1991; Zhang et al., 1991; Gaudemer et al., 1995; Guo et al., 2016) (Fig. 2A). The Cenozoic thrust systems in northern Tibet appear to be kinematically linked with the active >1000-km-long, east-striking Haiyuan, Qinling, and Kunlun left-slip faults (e.g., Taylor and Yin, 2009; Zuza and Yin, 2016), which accommodated significant Cenozoic shortening across northern Tibet (e.g., Gaudemer et al., 1995; Meyer et al., 1998; Wang and Burchfiel, 2004; Yin et al., 2007a, 2007b, 2008a, 2008b;

Zheng et al., 2010; Cheng et al., 2015; Allen et al., 2017; Yang et al., 2018; Zuza et al., 2019) (Fig. 1).

The early Paleozoic Qilian orogen, as summarized by Song et al. (2013) and Zuza et al. (2018), involved the collision of the Proterozoic Qaidam microcontinent with the Archean–Proterozoic North China craton to the north in the Ordovician–Silurian (e.g., Wu et al., 2016, 2017; Song et al., 2013; Zuza et al., 2018) (Fig. 2B). Jurassic and Cretaceous extensional and transtensional basin deposits are observed across northern Tibet and the Qilian Shan, from Xining Basin in the south to the Hexi Corridor in the north (e.g., Horton et al., 2004; Pan et al., 2004; Fang et al., 2019), which might have been associated with the closing of the Paleo-Tethys and Meso-Tethys Oceans and slab rollback to the south (e.g., Huo and Tan, 1995; Vincent and Allen, 1999; Chen et al., 2003; Yin et al., 2008a, 2008b; Pullen et al., 2008; Zhang et al., 2014; Wu et al., 2016, 2019b). The Cretaceous strata consist of pink conglomerate, sandstone, mudstone, and locally pyroxene andesite and tuffaceous sandstone interbedded with a thin layer of gypsum (e.g., Qinghai BGMR, 1991; Pan et al., 2004; Zuza et al., 2018; Chen et al., 2019a, 2019b), which are widely exposed near the Ebo and Qilian cities along the Hei River in the central Qilian Shan (Figs. 2B and 3).

The Qilian Shan has undergone tectonic deformation and uplift since the Eocene–Oligocene after the India-Asia collision, which formed the early Cenozoic Qilian Shan fold-thrust belt (e.g., Yin et al., 2008a, 2008b; Zuza et al., 2019; Li et al., 2019, 2020) (Fig. 2A). Northern Tibet and its foreland region, which includes the Hexi Corridor and the Longshou Shan regions, record protracted cooling since the Early Cretaceous (e.g., Jolivet et al., 2001; George et al., 2001; Li et al., 2019, 2020; An et al., 2020) (Table S1). This tectonic event reflects the enigmatic crustal uplift and shortening in the Early Cretaceous, which is consistent with the general absence of Cretaceous strata in the Qilian Shan and the occurrence of widespread early Cenozoic coarse-grained, alluvial sediments in the Hexi Corridor (e.g., Gansu BGMR, 1969; Vincent and Allen, 1999; Pan et al., 2004; Chen et al., 2019a, 2019b).

The Qilian Shan has undergone tectonic deformation and uplift since the Eocene–Oligocene after the India-Asia collision, which formed the early Cenozoic Qilian Shan fold-

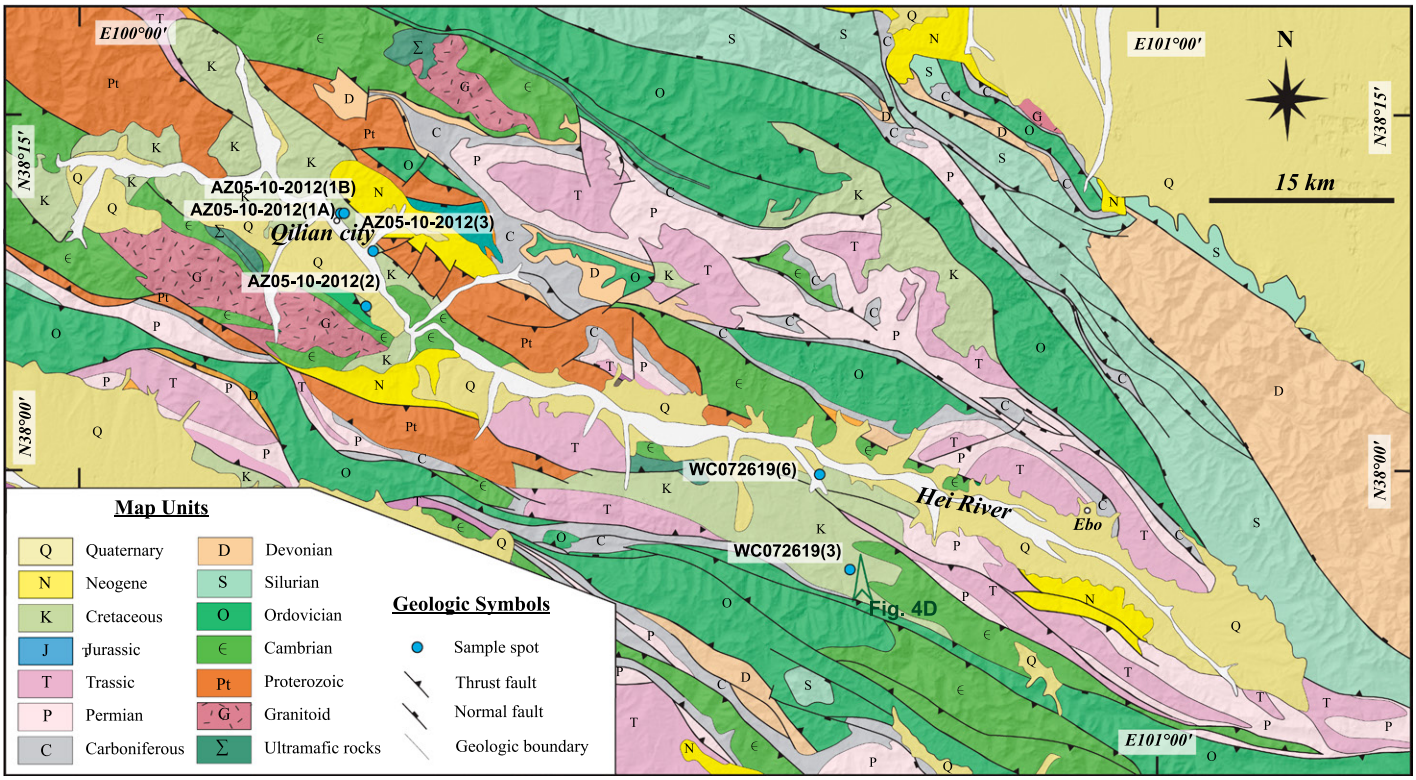

Figure 3. Field photos show the eastern Qilian Shan and Longshou Shan Proterozoic–Paleozoic granitoids and bedrocks. (A) Leucogranite dike intrudes the schist unit along the northeastern margin of the Xining Basin; the location of sample AZ09-12-2014 [1c] is shown. (B) Mesoproterozoic marble is thrust over Silurian slightly metamorphosed submarine sedimentary strata along a ~45° south-dipping fault near Menyuan; the location of sample WC09-13-2014 (10) is shown. (C) The lower Paleozoic sandstone unit is intruded by the Ordovician granitoid that is cut by the mafic dike; the location of sample WC09-14-2014 [15] is shown. (D) The structural relationship among the Ordovician, Carboniferous, and Cretaceous strata in the Qilian Shan; insets show the details as follows: (1) the Carboniferous strata interbedded with a coal layer are thrust over the Cretaceous red-colored, coarse-grained sandstone and (2) the Cretaceous reddish sandstone is tilted by the north-directed thrust; the location of sample WC072619 [3] is shown. (E–F) The Ordovician arc sequence is thrust over the Cretaceous sedimentary strata; the location of sample AZ05-10-2012 [2] is shown. (G) A pink granitoid pluton is thrust over the Mesoproterozoic quartoschist and meta-sandstone unit with the occurrence of a fault gouge; the location of sample WC09-15-2014 [4b] is shown. (H) A granite intrudes the schist unit in the eastern Longshou Shan; the location of sample WC09-16-2014 [5] is shown. (I) Devonian pink granitoid intrudes the Silurian-Devonian metagraywacke in the central Longshou Shan; the locations of samples WC09-17-2014 [2a] and WC09-17-2014 [2b] are shown.

thrust belt (e.g., Yin et al., 2008a, 2008b; Zuza et al., 2019; Li et al., 2019, 2020) (Fig. 2A). The Cenozoic Qilian Shan thrust belt initiated there shortly after the India-Asia collision in the Eocene (e.g., Clark et al., 2010; Yin et al., 2008a, 2008b; Duvall et al., 2011; Clark, 2012; Qi et al., 2016; Yu et al., 2017). However, significant exhumation and cooling in the Miocene, tracked via low-temperature thermochronology, suggests that Qilian Shan shortening accelerated in the Miocene (e.g., Pang et al., 2019; Yu et al., 2019b; Zheng et al., 2010, 2017; Zhuang et al., 2018; Wang et al., 2020a) (Table S1). The spatiotemporal deformation pattern in the Qilian Shan, Hexi Corridor, and Longshou Shan from late Mesozoic to the Cenozoic is poorly resolved; thus, it is necessary to improve our understanding of how the northern plateau developed (Fig. 2B). Due to a far-field effect and an increase in crustal thickness of the Tibetan Plateau during the India-Asia collision, the northern plateau has been interpreted to have expanded from the Qilian Shan thrust fault zone to the foreland region of the North China craton since the Miocene, which has been expressed by both thrusting and strike-slip faulting (e.g., Yuan et al., 2013; Duvall et al., 2013; Zuza et al., 2019; Chen et al., 2019a; An et al., 2020; Li et al., 2019, 2020) (Fig. 2A). Li et al. (2019) provided a direct initiation age constraint for the Cenozoic left-slip Haiyuan fault of 15–10 Ma based on a thermochronology traverse across a restraining bend (Fig. 2B) that formed by a ~20 km right step made by the strike-slip fault.

GEOLOGIC CONTEXT OF THE SAMPLING SITES

Our field observations show that the Proterozoic basement in the eastern Qilian Shan was intruded by granitoid dikes (Fig. 4A), which were thrust over the early Paleozoic submarine sedimentary strata along a ~45° south-dipping fault near Menyuan (Fig. 4B). An Ordovician granite pluton has a U-Pb zircon age of ca. 462 Ma (Zuza et al., 2018), which was cut by mafic dikes (Fig. 4C). Near the Ebo city, we observe that the Ordovician arc sequence and Carboniferous shallow marine sediments thrust over the Cretaceous fluvial lacustrine deposits (Fig. 4D), and the Cretaceous sandstone was tilted northward by north-directed thrusting (Fig. 4D). The structure may be associated with the development of the Haiyuan fault system; however, the deformation and exhumation history are unconstrained. Near the Qilian city, the early Paleozoic arc sequence thrust over the red-colored coarse sandstone and conglomerate unit (Figs. 4E and 4F).

The ~30-km-wide Longshou Shan is a northwest-trending, ~300-km-long range located in the Mesozoic–Cenozoic Hexi Corrdior foreland basin, west of the city of Jinchang, that is separate from the higher elevation Tibetan Plateau to the south (Fig. 2B). The range primarily exposes Proterozoic strata and metamorphic rocks that are thought to represent the southwestern margin of the North China craton (e.g., Bai and Dai, 1996; Tang and Bai, 2000; Gong et al., 2013, 2016) (Fig. 2B). Upper Paleozoic strata were deposited unconformably over Precambrian basement rocks and slightly metamorphosed Cambrian rocks (Zhang et al., 2016). Intra-continental foreland basin depositions were developed since the early Mesozoic. Proterozoic and early Paleozoic granitoids are widespread along the southern margin of the Longshou Shan (e.g., Zhang et al., 2016; Wang et al., 2020b), and were thrust over the metamorphic basement (Fig. 4G) or intrude Proterozoic metamorphic sedimentary (Fig. 4H) and/or Paleozoic metagraywacke (Fig. 4I). The present day range physiography and exposures are controlled by northwest-striking Cenozoic thrust faults. The northeastern range-bounding fault is active, and there is evidence for Cenozoic faulting throughout the Longshou Shan, including several east-striking, left-slip faults (Fig. 2B).

SAMPLES AND ANALYTICAL METHODS

Samples

Our approach for AFT sampling was to get diverse spatial coverage across the northeastern margin of the Tibetan Plateau. Low erosion and exhumation rates and a protracted Mesozoic–Cenozoic deformational history (e.g., Jolivet et al., 2001) complicates thermochronology campaigns and can yield a diverse range of ages. Therefore, this study conducted regional sampling across different domains of strike-slip and thrust-dominated fault structures (Fig. 2). Specifically, our traverse spanned from Qinghai Lake in the southwest, to the interior of the Qilian Shan to the Longshou Shan in the northeast, and off of the Tibetan Plateau. Samples were collected from both high-relief ranges that were presumably uplifting rapidly and intervening valleys that may reveal an earlier exhumation history. Previous studies focused on vertical traverses of thrust-belt margin ranges tend to get Miocene cooling ages (e.g., Zheng et al., 2010, 2017; Wang et al., 2020a), as is expected from rapidly exhuming active structures (Li et al., 2020), but our intent was to probe the prolonged Mesozoic–Cenozoic kinematic history of this region.

Twenty-three samples were collected from eastern Qilian Shan and Longshou Shan during the autumn of 2014 (Figs. 2B and 5A). Six Cretaceous sandstone samples were collected from the central Qilian Shan along the Hei River in different field campaigns in 2012 and 2019 (Figs. 3 and 5A). Samples, their locations, and specific rock types are shown in Table 1. Two Devonian samples WC 09-17-2014 (2a) and WC 09-17-2014 (2b) were collected from the southern margin of the central Longshou Shan (Fig. 5B). A Paleozoic granitoid sample WC 09-14-2014 (15) is from the northern margin of the eastern Qilian Shan (Fig. 5C), whereas volcanic sample AZ 09-15-2014 (3) is from the Hexi Corridor (Fig. 5D). Samples AZ09-15-2014 (6), AZ09-15-2014 (4a), WC09-15-2014 (4b), WC09-16-2014 (1a), WC09-16-2014 (1b), AZ09-16-2014 (3), AZ09-16-2014 (5), WC09-16-2014 (7a), WC09-16-2014 (7b), and AZ09-16-2014 (10) were collected from the Paleo- and Meso-Proterozoic basement rocks and Proterozoic intrusions at the eastern end of the Longshou Shan near Jinchang city (Fig. 5E). Proterozoic samples AZ09-12-2014 (1a), AZ09-12-2014(1b), and AZ09-12-2014(2b) were collected from the northeastern margin of the Xining basin (Fig. 5F). The six Cretaceous, red-colored, coarse sandstone samples AZ 05-10-2012 (1A), AZ 05-10-2012 (1B), AZ 05-10-2012 (2), AZ 05-10-2012 (3), WC072619(3), and WC072619(6) are from the Hei River (Fig. 5G) and were part of the footwall rocks of major Qilian Shan thrust faults. Near Menyuan city, samples AZ 09-13-2014 (3), WC 09-13-2014 (7), WC 09-13-2014 (8c), AZ 09-13-2014 (9a), and WC 09-13-2014 (9b) were located at the hanging wall of the Menyuan thrust, whereas the Paleozoic sandstone sample WC 09-13-2014 (10) was in the footwall (Figs. 4B and 5H).

AFT Analyses

Fission-track thermochronology is based on crystal-lattice damage that is manifested as linear tracks that developed as a result of the constant spontaneous fission of trace levels of ^{238}U in zircon and apatite grains. Fission tracks in apatite are incompletely annealed over the temperature range of ~60–120 °C, which is termed the partial annealing zone (PAZ) (e.g., Gleadow, 1981; Gleadow et al., 2002; Ketcham et al., 2007). Cooling of a sample through the partial annealing zone with time is reflected by the distribution of lengths of the partially annealed tracks. We conducted apatite fission-track (AFT) analyses of 29 samples to determine the low-temperature thermal history of the Qilian Shan-Longshou Shan (Figs. 2B and 5).

Figure 4. Regional geological map shows the area along the Hei River (modified from Qinghai BGMR, 1991, and our field observations). Underlying base map is from www.geomapapp.org (accessed January 2021; Ryan et al., 2009). The original field pictures show Figure S1 (see footnote 1).

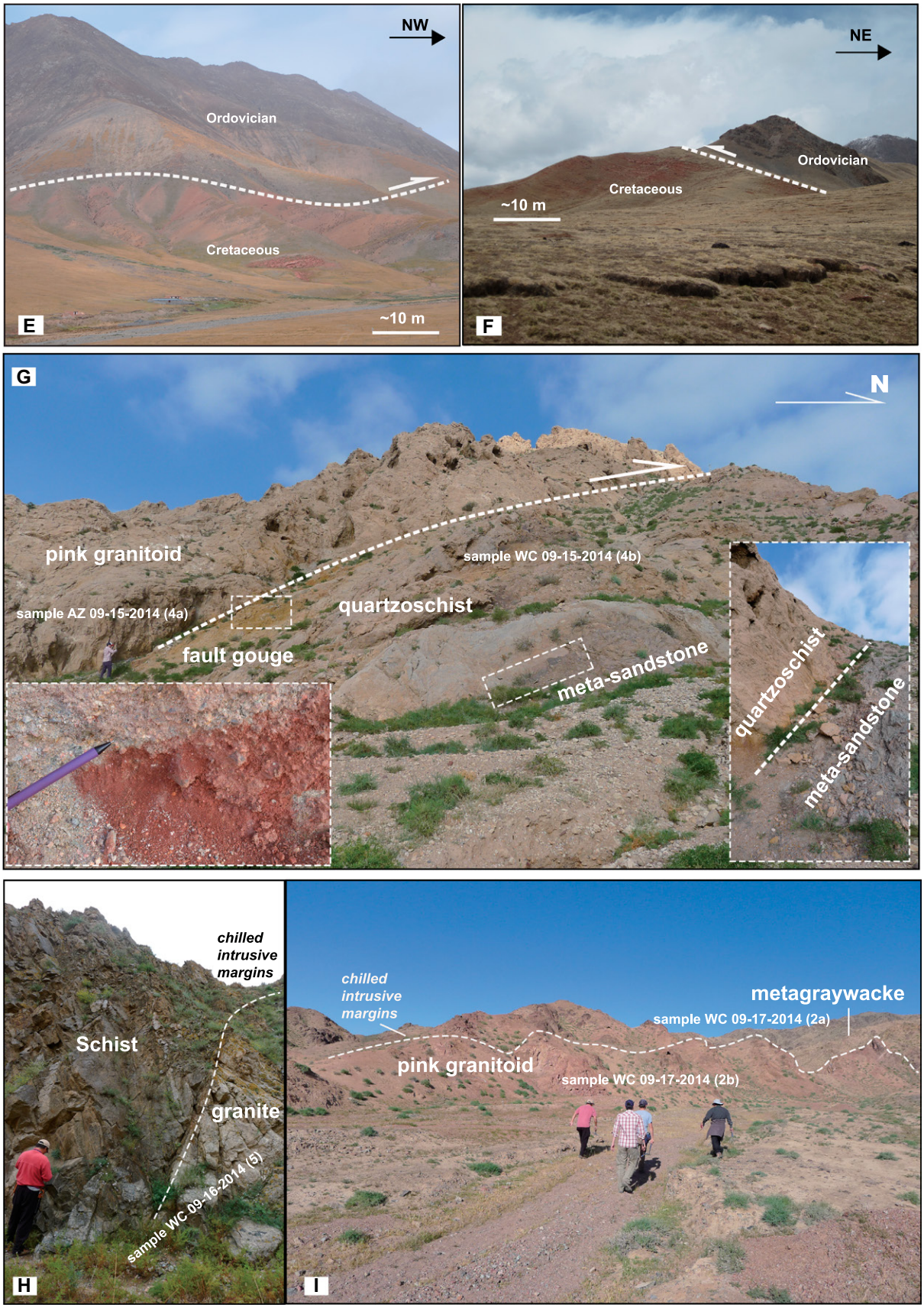

Figure 4. (continued)

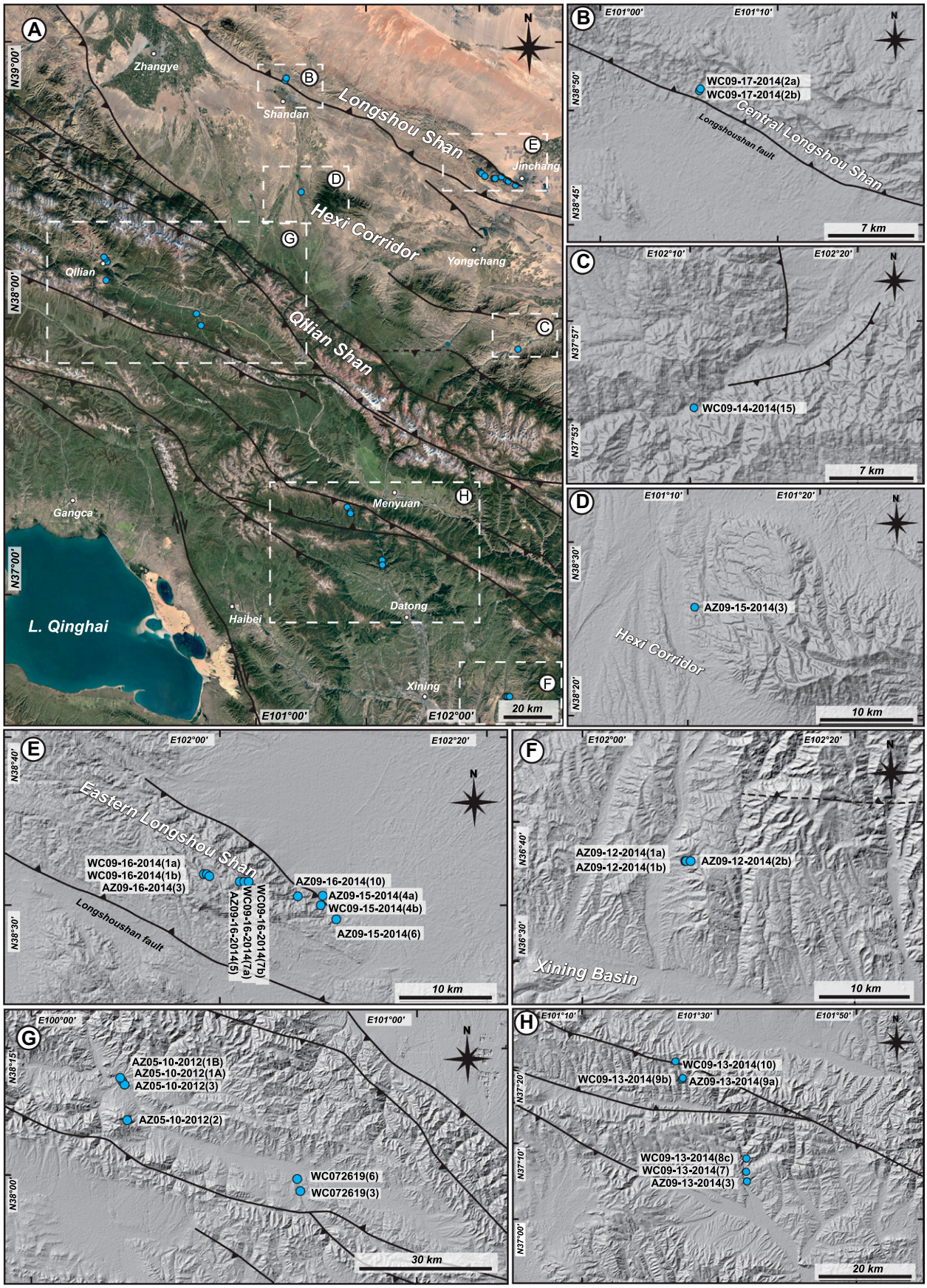

Figure 5. Satellite images of the eastern Qilian Shan and Longshou Shan show (A) sample locations of the apatite fission-track samples including (B) the central Longshou Shan, (C) northeastern margin of the Qilian Shan, (D) Hexi Corrdior, (E) eastern Longshou Shan, (F) eastern margin of the Xining basin, (G) Cretaceous sandstone samples along the Hei River, and (H) area near Menyuan and the northern margin of the Xining basin.

Fission-track ages were measured using the external detector method (Gleadow, 1981) and calculated using the zeta calibration method (Hurford and Green, 1983). Ages were calculated using the Zeta calibration method (Hurford and Green, 1983; Hurford, 1990) with a Zeta value of 322.1 ± 3.6 (1 s). Apatite grains were separated from ~5 kg of material from each sample using standard mineral separation techniques. Polished grain mounts were prepared and etched to reveal spontaneous fission tracks. Apatite grain mounts were etched in 6.6% HNO_3 at 25 °C for 30 seconds. All samples were irradiated at the China Institute of Atomic Energy reactor facility, Beijing. Low-U muscovite external detectors covering apatite grain mounts were etched in 40% hydrofluoric acid at 25 °C for 20 min to reveal induced fission tracks. To increase the number of observable horizontal confined tracks, the samples were exposed to ^{252}Cf (Donelick and Miller, 1991). Horizontally confined fission-track lengths (e.g., Laslett et al., 1987; Gleadow et al., 1986) were measured only in prismatic apatite crystals because of the anisotropy of annealing of fission tracks in apatite (Green et al., 1986).

Thermal History Modeling

Because fission-track systematics in apatite are characterized by a PAZ approximately between 60 °C and 120 °C, AFT ages and measured fission-track length distributions can be inverted to produce suites of compatible thermal histories. We performed inverse modeling of the AFT data using the HeFTy v1.9.1 software of Ketcham (2005) and the kinetic annealing model for apatite of Ketcham et al. (2007) that considers the Dpar values and the angle with c-axis parameters. Goodness-of-fit (GOF) value was used to estimate how well the modeled data fit measured values (Ketcham, 2005). The paths were accepted (green envelopes) when GOF was > 0.05 and rated as good (pink envelopes) for GOF > 0.5 (Ketcham, 2005). Inverse thermal history modeling was run for 100,000 paths for each sample, which in all cases resulted in at least 1000 acceptable paths.

TABLE 1. APATITE FISSION-TRACK ANALYTICAL RESULTS FOR THE LONGSHOU SHAN AND QILIAN SHAN FROM THIS STUDY

Sample	Latitude (°N)	Longitude (°E)	Elevation (m)	Grains	ρ_s (10^5/cm^2)	Ns	ρ_i (10^5/cm^2)	Ni	ρ_d (10^5/cm^2)	Nd	P(χ^2) (%)	Pooled age (± 1σ Ma)	Central age (± 1σ Ma)	Mean track length (μm)	Nj	Average Dpar (μm)	Lithology	modeling good path
AZ09-12-2014(2b)	36.63025	102.1496167	2697	10	2.367	114	5.398	260	10.839	5474	37.5	92 ± 11	91 ± 12	12.3 ± 2.2	15	1.31	gneiss	yes
AZ09-12-2014(1b)	36.63105	102.1360167	2566	30	9.559	1901	19.335	3845	12.873	5474	0.4	123 ± 7	122 ± 8	12.0 ± 2.1	206	1.46	granitoid	yes
AZ09-12-2014(1a)	36.63105	102.1360167	2566	35	3.784	1113	7.606	2237	13.612	5474	30.7	131 ± 8	131 ± 8	12.2 ± 1.8	123	1.36	schist	yes
AZ09-13-2014(3)	37.089978	101.5663	2617	35	5.56	1303	11.001	2578	12.133	5474	78.6	119 ± 7	119 ± 7	13.4 ± 1.8	115	1.31	diorite	yes
WC09-13-2014(7)	37.110339	101.568875	2724	30	11.968	2727	27.657	6302	13.242	5474	11.1	111 ± 6	111 ± 6	12.0 ± 1.8	284	1.54	gneiss	no
WC09-13-2014(8c)	37.13575	101.5700167	2685	35	0.551	100	1.796	326	11.394	5474	100	68 ± 8	68 ± 8	12.0 ± 2.5	79	1.44	basalt	yes
WC09-13-2014(9b)	37.30011667	101.4198167	3244	35	4.102	1411	12.537	4312	13.612	5474	26.8	87 ± 5	86 ± 5	12.3 ± 1.7	130	1.23	marble	no
AZ09-13-2014(9a)	37.30011667	101.4198167	3244	35	19.526	2119	46.866	5086	10.655	5474	0.9	86 ± 5	86 ± 5	12.0 ± 2.2	194	1.35	leucogranite	no
AZ09-13-2014(10)	37.32485	101.40095	3584	35	4.616	1657	17.95	6444	12.873	5474	0	64 ± 4	64 ± 4	11.9 ± 2.1	146	1.30	sandstone	yes
WC09-14-2014(15)	37.88925	102.17285	2101	30	9.608	3234	38.315	12896	12.506	5474	0	61 ± 3	61 ± 3	11.8 ± 2.2	209	1.55	granitoid	yes
AZ09-15-2014(3)	38.44286667	101.17115	1621	35	0.685	259	1.343	508	12.133	5474	90.7	120 ± 11	120 ± 11	13.2 ± 2.0	120	1.55	metavolcanic	yes
AZ09-15-2014(6)	38.4817	102.1515333	1675	35	4.374	943	14.288	3080	13.612	5474	0	81 ± 5	74 ± 6	12.3 ± 2.2	133	1.38	leucogranite	no
WC09-15-2014(4b)	38.49585	102.1297833	1639	35	0.91	206	3.628	821	10.47	5474	25.6	51 ± 5	43 ± 6	12.9 ± 1.8	64	1.33	quartzoschist	yes
AZ09-15-2014(4a)	38.49585	102.1297833	1639	35	0.194	43	1.351	299	11.394	5474	99.4	32 ± 5	32 ± 5	11.9 ± 2.2	32	1.21	granitoid	yes
WC09-16-2014(7b)	38.50358333	102.0829	1853	35	4.204	1150	13.821	3781	12.873	5474	2.3	76 ± 4	76 ± 5	12.2 ± 2.0	144	1.49	paragneiss	no
WC09-16-2014(7a)	38.50358333	102.0829	1853	28	11.405	6638	32.608	18979	13.612	5474	0	92 ± 5	91 ± 6	12.0 ± 2.1	223	1.33	orthogneiss	no
AZ09-16-2014(5)	38.5062	102.06845	1922	35	3.204	962	7.845	2355	10.839	5474	93.7	86 ± 5	86 ± 5	12.5 ± 1.6	124	1.39	granitoid	no
AZ09-16-2014(3)	38.50988333	102.05115	2003	35	0.431	73	2.25	381	11.394	5474	99.4	43 ± 6	43 ± 6	12.1 ± 2.0	72	1.31	granitoid	no
AZ09-16-2014(10)	38.51145	102.09825	1750	35	0.558	92	2.073	342	12.133	5474	100	64 ± 8	64 ± 8	12.7 ± 2.0	58	1.54	leucogranite	yes
WC09-16-2014(1b)	38.51153333	102.0470167	2033	35	6.877	1548	17.072	3843	12.133	5474	59	95 ± 5	95 ± 5	12.1 ± 2.0	151	1.39	quartzoschist	yes
WC09-16-2014(1a)	38.51153333	102.0470167	2033	35	2.026	681	9.498	3192	12.873	5474	0	54 ± 3	54 ± 5	11.8 ± 2.2	110	1.35	quartzite	yes
WC09-17-2014(2b)	38.85035	101.0966833	1976	42	0.202	41	1.607	326	10.655	5474	97.6	26 ± 5	26 ± 5	–	–	–	granitoid	/
WC09-17-2014(2a)	38.85035	101.0966833	1976	30	8.744	2845	21.308	6933	11.394	5474	18.3	91 ± 5	91 ± 5	12.4 ± 1.9	256	1.35	metagraywacke	yes
Six Cretaceous sandstone samples																		
WC072619(3)	37.9657	100.697908	3221	35	5.267	716	17.256	2346	11.394	5474	0	68 ± 4	67 ± 7	11.8 ± 2.4	129	1.94	Sandstone	yes
WC072619(6)	37.989008	100.68635	3185	35	2.65	569	13.024	2796	12.133	5474	0	48 ± 3	47 ± 4	11.6 ± 2.5	105	1.47	Sandstone	yes
AZ05-10-2012(2)	38.177842	100.254722	3881	35	1.201	535	12.688	5650	12.688	5474	0	23 ± 2	27 ± 3	11.8 ± 2.3	91	1.46	Sandstone	yes
AZ05-10-2012(3)	38.180233	100.255347	2773	35	1.296	480	26.642	9868	10.655	5474	53.8	10 ± 1	10 ± 1	12.8 ± 2.1	46	1.40	Sandstone	yes
AZ05-10-2012(1A)	38.187167	100.2505	2761	36	0.919	213	4.929	1142	13.797	5474	29.1	50 ± 4	52 ± 6	10.0 ± 1.3	26	1.34	Sandstone	yes
AZ05-10-2012(1B)	38.187167	100.2505	2761	35	0.666	82	4.019	495	13.242	5474	3.7	43 ± 6	48 ± 7	–	–	1.21	Sandstone	/

Note: Track densities are ($\times 10^6$ tr cm^{-2}) and the number of tracks counted (N) is shown in parentheses.

We divide the samples into two groups for discussion and thermal modeling based on their geologic setting. The 23 analyses of Proterozoic–Paleozoic samples from the eastern Qilian Shan and Longhsou Shan were collected from rocks that were mostly likely at depths >5 km prior to the Mesozoic based on their geologic histories and lithology (e.g., intrusions or even amphibolite-grade metamorphic rocks), and thus we assume that the samples started at temperatures equal to, or hotter than, the AFT PAZ (~60–120 °C). The Cretaceous strata from which six samples were collected have maximum thicknesses of ≤1.4 km (e.g., Qinghai BGMR, 1991; Pan et al., 2004; Zuza et al., 2018). Therefore, the analyzed apatite grains in the Cretaceous sediments would have been deposited at depths shallower than the AFT PAZ. For all samples except the Cretaceous samples (i.e., the Proterozoic–Paleozoic samples), initial time–temperature conditions were set at above the AFT PAZ at a time range of 200–50 Ma. This initial condition is justified because all of these studied rock types are thought to have originated from below the uppermost crust. Therefore, the thermal modeling started with the AFT samples above the AFT PAZ in the Cretaceous and sought to see what temperature–time paths were permissible for the samples studied and included the possibility of reheating via post-depositional tectonic burial. The thermal history model inputs for simulations are in Table 2 (e.g., Flowers et al., 2015).

RESULTS AND INTERPRETATIONS

AFT Results

The results of AFT analyses of our Qilian Shan-Longshou Shan samples are shown in Table 1 and include AFT age, track length, and Dpar information. We used the central age of these samples. For the remaining AFT samples that passed the chi-square test, pooled AFT ages are reported (e.g., Sobel et al., 2006a, 2006b; Donelick et al., 2005; Cao et al., 2015; Table 1). AFT ages from 23 Proterozoic–Paleozoic samples from the eastern Qilian and Longshou Shan are spread over a wide range from 131 ± 8 Ma (eastern Qilian Shan sample AZ 09-12-2014 [1a]) to 26 ± 5 Ma (central Longshou Shan sample WC 09-17-2014 [2b]) with Dpar values of 1.21–1.55 (Table 1). Twelve Longshou Shan samples yield AFT ages ranging from 95 ± 5 Ma (sample WC 09-16-2014 [1b]) to 26 ± 5 Ma (sample WC 09-17-2014 [2b]), whereas one Hexi Corridor sample AZ 09-15-2014 (3) yields an AFT age of 120 ± 11 Ma (Table 1). The other 10 eastern Qilian Shan samples yield AFT ages ranging from 131 ± 8 Ma (sample AZ09-12-2014 [1a]) to 61 ± 3 Ma (sample WC 09-14-2014 [15]) (Table 1). The six Cretaceous sandstone samples yield AFT ages spanning 68 ± 4 Ma (sample WC072619[3]) to 10 ± 1 Ma (AZ 05-10-2012 [3]) with Dpar values of 1.34–1.94 (Table 1).

The mean track lengths of our Proterozoic–Paleozoic AFT samples range from 11.8 ± 2.2 μm (samples WC 09-14-2014 [15] and WC 09-16-2014 [1a]) to 13.4 ± 1.8 μm (sample AZ 09-13-2014 [3]) (Table 1). The mean track lengths of our Cretaceous AFT samples range from 12.8 ± 2.1 μm (sample AZ 05-10-2012 [3]) to 11.6 ± 2.5 μm (sample WC072619 [6]) (Table 1). These track-length distributions generally suggest that the tracks were shortened by annealing, possibly during long-term annealing-related residence in the PAZ (e.g., Gleadow et al., 1986; Green, 1988). Almost all AFT ages were significantly younger than their respective crystallization or depositional ages (Table 1), which suggests that samples have experienced post-crystallization or post-depositional cooling histories through the apatite PAZ (e.g., Galbraith and Laslett, 1993; Gallagher et al., 1998; Yuan et al., 2006a, 2006b). Only Cretaceous sample WC072619 (3) yielded an AFT age of ca. 69 Ma, which was close to, but still younger than, the depositional age for this sample (e.g., Qinghai BGMR, 1991; Pan et al., 2004; Zuza et al., 2018).

Results from 16 of the AFT samples passed the chi-square test (P (χ2) > 5%; Fig. 6). Twelve of the samples (i.e., samples AZ 09-13-2014 [9a], AZ 09-13-2014 [10], WC 09-14-2014 [5], AZ 09-15-2014 [6], WC 09-16-2014 [1a], WC 09-16-2014 [7a], WC 09-16-2014 [7b] and five Cretaceous sandstone samples; Table 1) failed the chi-square test (P (χ2) < 5%; Galbraith and Green, 1990), which indicates significant dispersion in the individual grain ages of these samples (Fig. 6). The variable single grain ages of the AFT samples have been observed in another region of northern Tibet (e.g., Lin et al., 2011; Craddock et al., 2014; Zheng et al., 2017; He et al., 2018; Li et al., 2019, 2020; Yu et al., 2019a, 2019b; An et al., 2020; He et al., 2020), and age distribution probably reflects complex structural locations (e.g., Cao et al., 2013, 2021). All of our Cretaceous sandstone samples failed the χ2 test, which indicates their mixed grain age distributions (Fig. 6).

The observed grain age distributions were decomposed into different grain age components for these samples using the DensityPlotter program (Vermeesch, 2012; Fig. 7). The modeled peak ages of these age components from 10 eastern Qilian Shan samples are grouped into four populations based on their peak age

Figure 6. Apatite fission-track radial plots of the study samples from RadialPlotter are by Vermeesch (2009).

TABLE 2. THERMAL HISTORY MODEL INPUT FOR SIMULATIONS OF EASTERN QILIAN SHAN AND LONGSHOU SHAN APATITE FISSION TRACK (AFT) DATA

1. Apatite fission track data: Samples and data used in simulations	
Data type	Data source
AFT single grain ages and individual track lengths Treatment: each bedrock sample was counted as a separated constraint in HeFTy Error (Ma) applied in modeling: the 1σ sample standard deviation of each sample was applied	This study (Table 1)
2. Additional geologic information	
Assumption	Explanation and source
Initial condition began at a high temperature of 160–200 °C	Available AFT data indicated complete apatite annealing at this high temperature
AFT ages were set through the apatite PAZ temperature range of 60–110 °C	The AFT system is especially sensitive to this temperature range (~60–110 °C; Gleadow and Duddy, 1981)
Surface temperature of 20 ± 5 °C was reached by0 Ma	Average surface temperature is end-member minimum estimate.
3. System- and model-specific parameters	
Modeling Code: HeFTy v1.9.1 FT annealing model: Multi-kinetic annealing model of Ketcham et al. (2007); the Dpar values and the angle with C-axis parameters were applied. Statistical fitting criteria: GOF values > 0.05 for accepted fit; GOF values > 0.5 for good fit; Number of t–T paths attempted: >10,000 for each sample t–T path characteristics: reheating allowed after AFT age.	

Note: deposit age was used as the initial condition at the surface temperature for samples AZ05-10-2012(1A), AZ05-10-2012(2), AZ05-10-2012(3), WC072619(3) and WC072619(6). PAZ—partial annealing zone; GOF—goodness of fit.

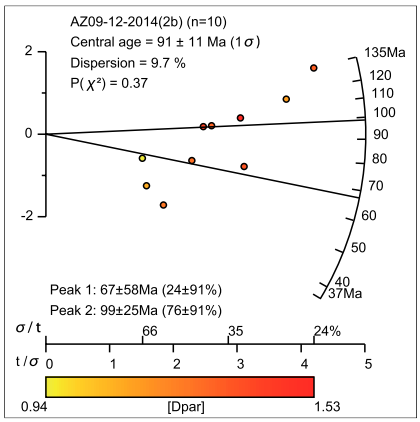

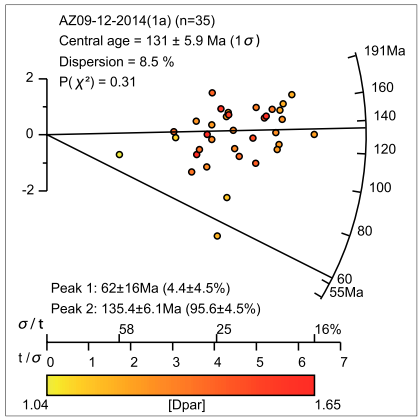

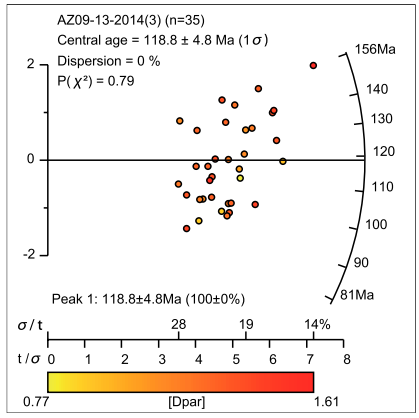

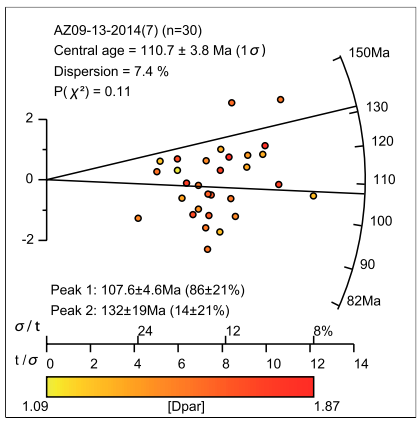

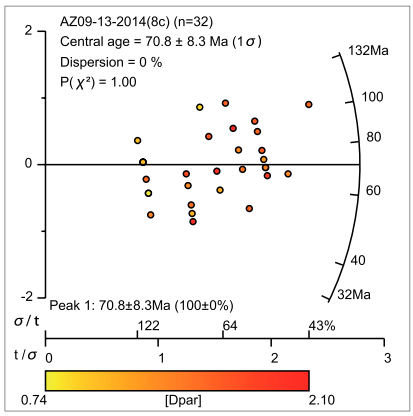

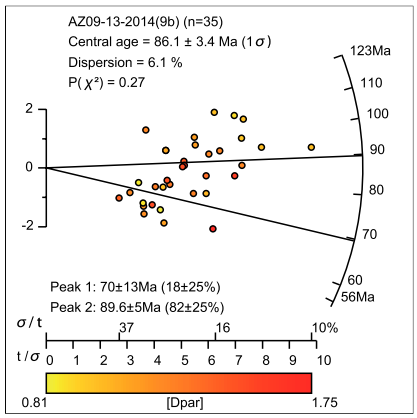

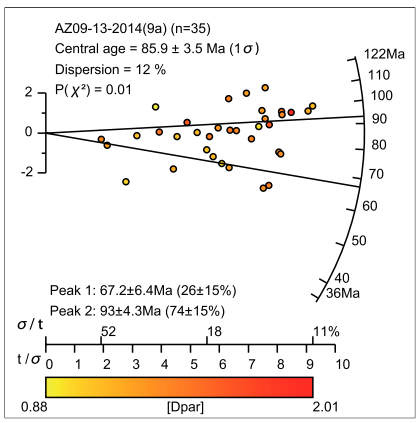

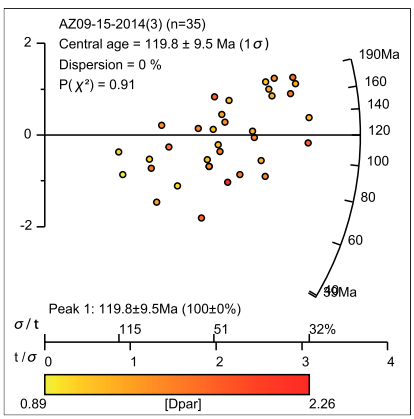

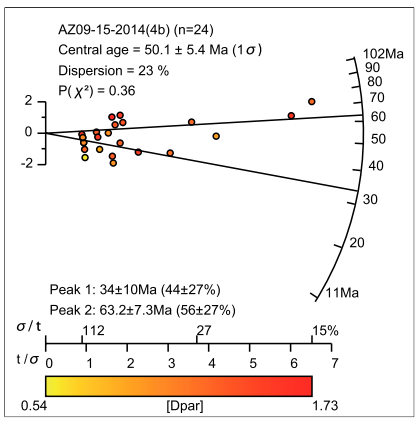

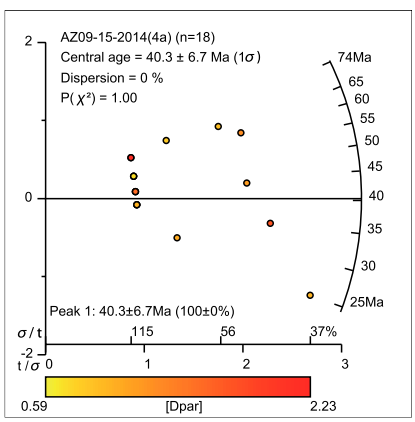

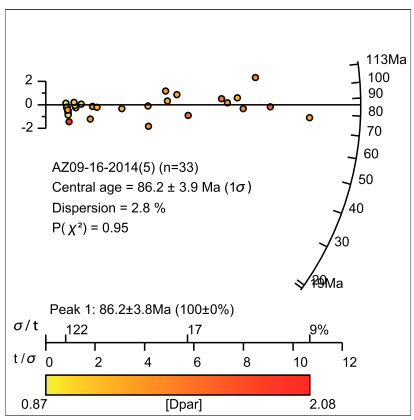

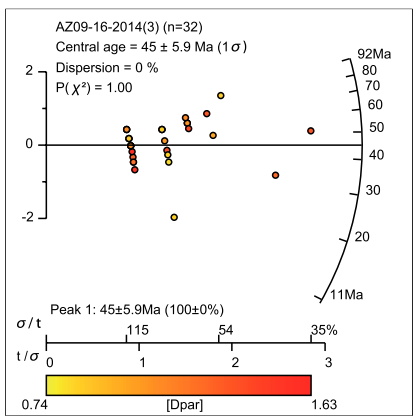

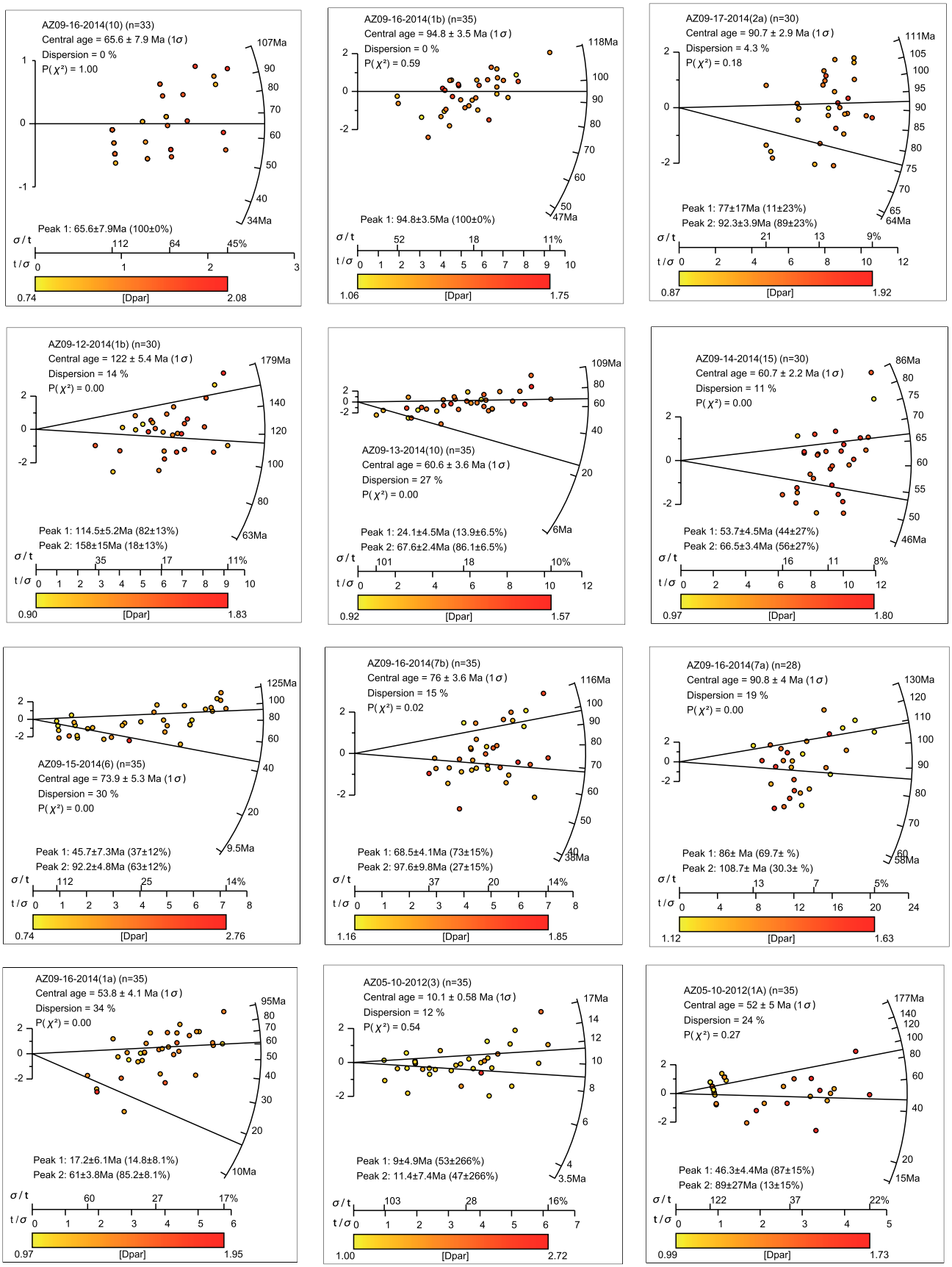

Figure 6. (continued)

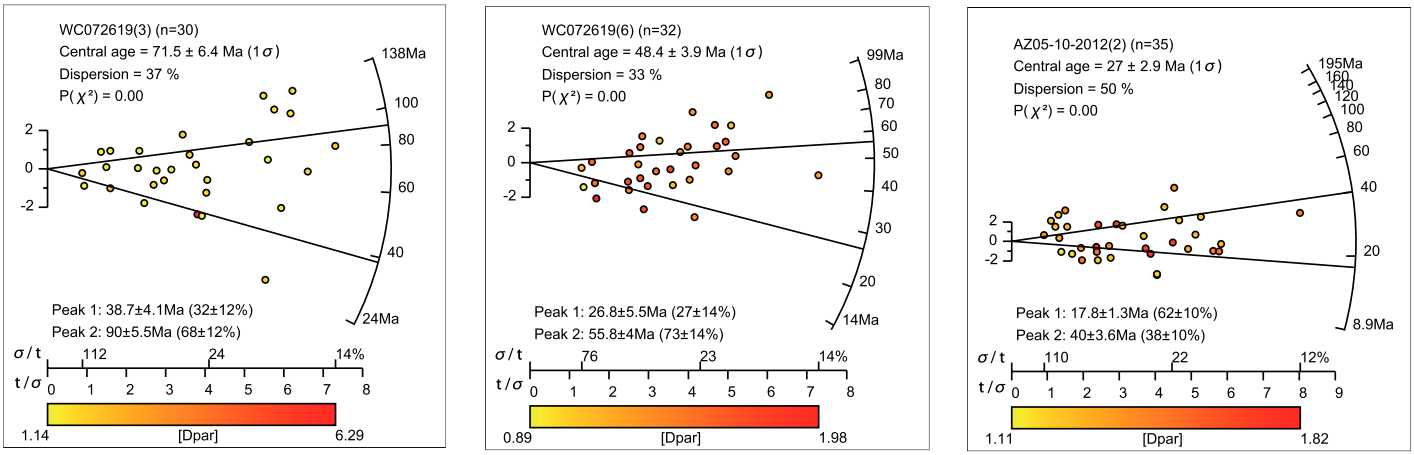

Figure 6. (continued)

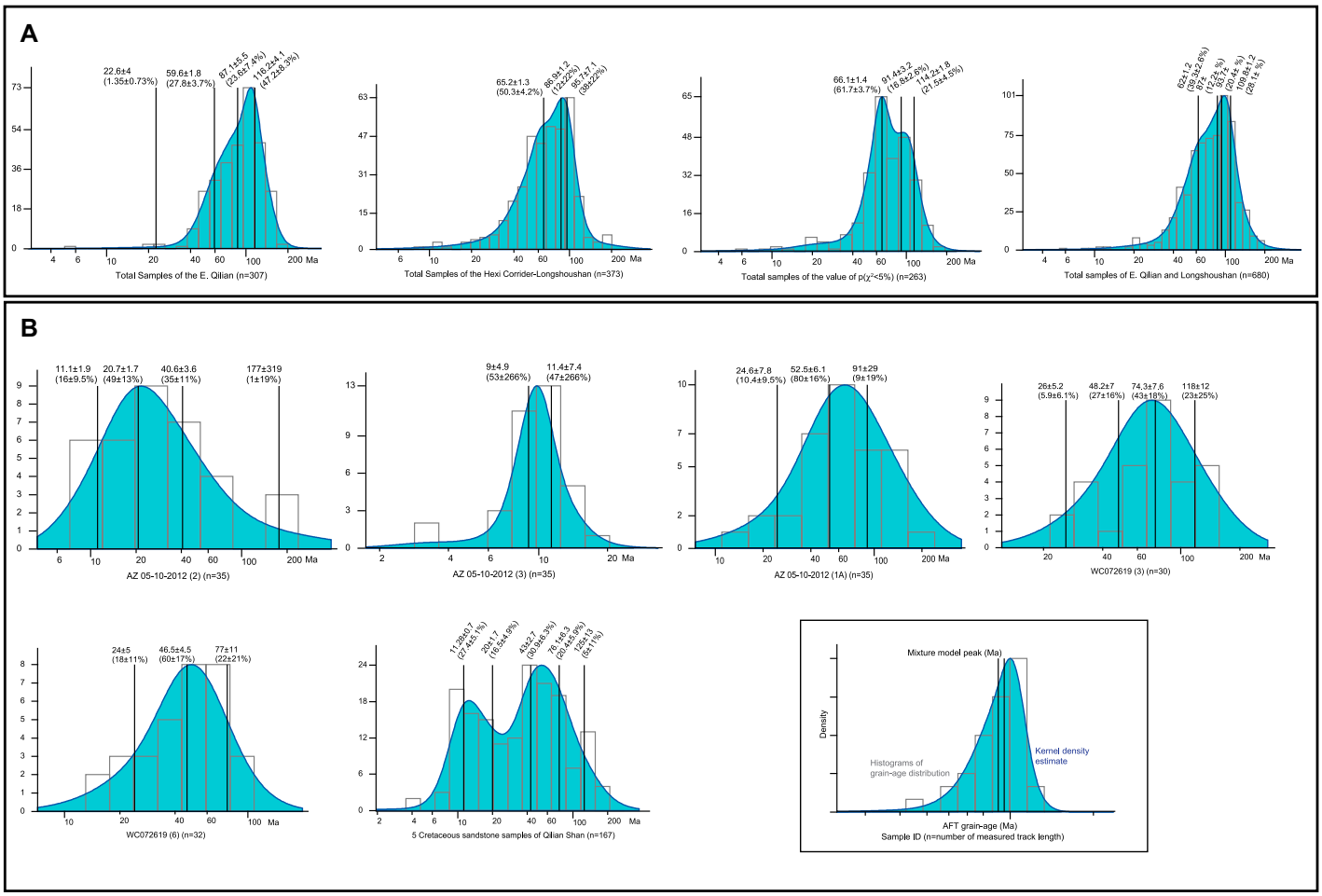

Figure 7. Grain age distributions and kernel density estimates of apatite fission-track (AFT) ages of the study samples are shown. (A) Proterozoic–Paleozoic samples from the eastern Qilian Shan and Longshou Shan; (B) Cretaceous sandstone samples in the footwall of the Cenozoic thrust along the Hei River.

correlations, which are termed P1 (ca. 22.6 Ma), P2 (ca. 59.6 Ma), P3 (ca. 87.1 Ma), and P4 (ca. 116.2 Ma), respectively. This demonstrates that multi-phase cooling affected the eastern Qilian Shan since the Early Cretaceous to Miocene (Fig. 7A). Three AFT age populations are observed from the 12 Hexi Corridor-Longshou Shan samples with age peaks of ca. 65.2 Ma, ca. 86.9 Ma, and ca. 95.7 Ma, which supports a cooling history that affected the Longshou Shan during the Late Cretaceous (Fig. 7A). The five Cretaceous strata yielded five age populations,

termed P1 (ca. 11 Ma), P2 (ca. 20 Ma), P3 (ca. 43 Ma), P4 (ca. 76 Ma), and P5 (ca. 125 Ma) (Fig. 7B). The peak ages of every component in each sample are younger than the corresponding depositional ages, and all single-grain ages and peak ages of decomposed components are not regarded to reflect pre-depositional cooling in their source terranes (e.g., van der Beek et al., 2006; Lin et al., 2015; Li et al., 2019; He et al., 2020). We combined the remaining samples that failed the χ^2 test, which displayed age peaks of 62.0–66.1 Ma, 93.7–87.0 Ma, and 114.2–109.8 Ma. These age peaks demonstrate that the multi-phase rapid cooling affected the eastern Qilian Shan-Longshou Shan region during the Cretaceous (Fig. 7A).

Thermal Modeling

Thermal history modeling of the AFT ages, track lengths, and Dpar data is used to evaluate the cooling processes and was conducted using the HeFTy program to produce time–temperature pathway models in this study (Ketcham, 2005; Ketcham et al., 2007, 2009). Nineteen samples yield good thermal modeling results, of which seven are from the eastern Qilian Shan, five Cretaceous samples are from the central Qilian Shan, and seven are from the Hexi Corridor-Longshou Shan. These models provide constraints on the exhumation history of the northeasternmost plateau (Fig. 8). Ten samples were not modeled because they were either missing mean track length data (samples WC09-17-2014 [2b] and AZ05-10-2012 [1b]) or did not yield any satisfactory model paths (samples WC09-13-2014 [7], WC09-13-2014 [9b], AZ09-13-2014 [9a], AZ09-15-2014 [6], WC09-16-2014 [7a], WC09-16-2014 [7b], AZ09-16-2014 [3], AZ09-16-2014 [5], and WC09-17-2014 [2b]) (Table 1).

Three samples from the eastern margin of the Xining basin (AZ09-12-2014 [1a], AZ09-12-2014 [1b], and AZ09-12-2014 [2b]) were cooled from a temperature above the upper limit of the AFT PAZ during the Early–Middle Jurassic, followed by thermal stagnation in the PAZ through its lower limit and accelerated cooling at ca. 25 Ma to the surface (Fig. 8A). Two samples collected from the northern margin of the Xining basin (AZ09-13-2014 [3] and WC09-13-2014 [8c]) had experienced initial cooling into the AFT PAZ since the Middle Jurassic, subsequent long-term tectonic quiescence in the PAZ, and finally rapid cooling through the lower limit of the PAZ since ca. 30 Ma (Fig. 8A). Sample AZ09-13-2014 (10), collected from the footwall of the Menyuan thrust fault (Fig. 4B), cooled through the PAZ during the Jurassic and has cooled from the PAZ to the surface since the Early Cretaceous (Fig. 8A). One sample, WC09-14-2014 (15), collected from the northeastern margin of the Qilian Shan, is characterized by initial Late Cretaceous cooling, residence within the PAZ, and finally a strong pulse of rapid cooling through the lower limit of the PAZ since ca. 12 Ma (Fig. 8A).

All Cretaceous samples yielded Cenozoic AFT ages except for sample WC072619 [3] (Late Cretaceous, 68 ± 4 Ma). Given that these samples were deposited at depths of <1.4 km in the Cretaceous (e.g., Qinghai BGMR, 1991; Pan et al., 2004; Zuza et al., 2018), these mostly Cenozoic ages imply that the samples were heated to AFT PAZ conditions (e.g., implied burial depths of ~2–6 km based on 20–30 °C/km geothermal gradients) after Cretaceous deposition but prior to their middle–late Cenozoic exhumation. The track length distributions for these samples have wide and low amplitude, which is consistent with reheating and/or long residence within the AFT PAZ (Table 1; e.g., Gleadow et al., 1986; Green, 1988). Thermal history modeling supports this overall interpretation. All samples show required heating to AFT PAZ temperatures in the late Mesozoic or early Cenozoic and variable residence in the PAZ (Fig. 8B). The time–temperature evolution of this required late Mesozoic to early Cenozoic reheating is entirely unconstrained especially after deposition and before the AFT ages and thermal models portray cooling out of the AFT PAZ. The analyzed Cretaceous samples experienced cooling from the AFT PAZ to surface temperatures in the Miocene to present timeframe (Fig. 8B).

The Hexi Corridor Devonian sample AZ09-15-2014 (3) shows paths of rapid cooling from a temperature above the upper limit of the AFT PAZ during the Middle Jurassic, residence within the PAZ, and finally rapid cooling through the lower limit of the PAZ since the Late Cretaceous (Fig. 8C). The thermal histories from four eastern Longshou Shan samples (AZ09-15-2014 [4a], WC09-16-2014 [1a], WC09-16-2014 [1b], and AZ09-16-2014 [10]) reflect the variable cooling process from the Early Jurassic to present (Fig. 8C). At ca. 200–180 Ma, a relatively rapid cooling stage occurred with a corresponding crustal temperature decrease of ~50 °C from ~170 °C to ~120 °C and a cooling rate of ~2.5 °C/Ma. The next stage, at ca. 180–90 Ma, experienced a subsequent long-term tectonic quiescence in the PAZ. The third stage displayed rapid cooling from ca. 90 Ma to ca. 60 Ma with a commensurate temperature decrease of ~90–60 °C and a cooling rate of ~1.0 °C/Ma and finally rapid exhumation from ca. 20 to present, which was accompanied by a temperature decrease from ~60 °C to the present surface temperature of ~20 °C with a cooling rate of ~2.0 °C/Ma. However, the footwall sample WC 09-15-2014 (4b) reveals cooling in the Jurassic to the Late Cretaceous to the bottom of the AFT PAZ, which was followed by thermal stagnation in the PAZ and cooling from the PAZ to the surface since the early Cenozoic (Fig. 8C). One graywacke sample AZ09-17-2014 (2a) from the central Longshou Shan exhibits cooling from a temperature above the upper limit of the AFT PAZ during the Cretaceous and residence in the PAZ until it was cooled rapidly through the lower limit of the PAZ since 25 Ma (Fig. 8C).

DISCUSSION

In this study, the AFT data presented from the Qilian Shan-Longshou Shan record the cooling timing and rate of upper crust exhumation and tectonic activity during the late Mesozoic and Cenozoic (Figs. 8 and 9). With detailed field observations and the structure positions of these thermochronologic samples, we further constrain the deformation history of the northern Tibetan Plateau and foreland region by exploring the structural and exhumation histories. Most previous studies have focused on Cenozoic deformation shortly after the initial India-Asia collision at ca. 55–58 Ma, but the late Mesozoic exhumation history observed in this study has important implications for the growth history of the northern plateau. Our AFT analyses and thermal history modeling demonstrate that the Qilian Shan and Longshou Shan experienced a complex, multi-phase cooling history through the late Mesozoic to the Cenozoic (Figs. 8 and 9).

Thermal and Tectonic History of the Eastern Qilian Shan

The thermal models of our eastern Qilian Shan samples suggest three significant cooling events since the Late Jurassic–Early Cretaceous, during or since the Eocene, and since the middle Miocene (Fig. 9A). The Late Jurassic–Early Cretaceous cooling event recorded by our AFT results in the eastern Qilian Shan corresponds

Figure 8. Apatite fission-track thermal history models and length distributions derived using HeFTy software (Ketcham, 2005) are shown. (A) Proterozoic–Paleozoic samples in the eastern Qilian Shan; (B) Cretaceous samples in the central Qilian Shan; (C) Proterozoic–Paleozoic samples in the Longshou Shan. PAZ—partial annealing zone.

A Proterozoic-Paleozoic samples in the eastern Qilian Shan

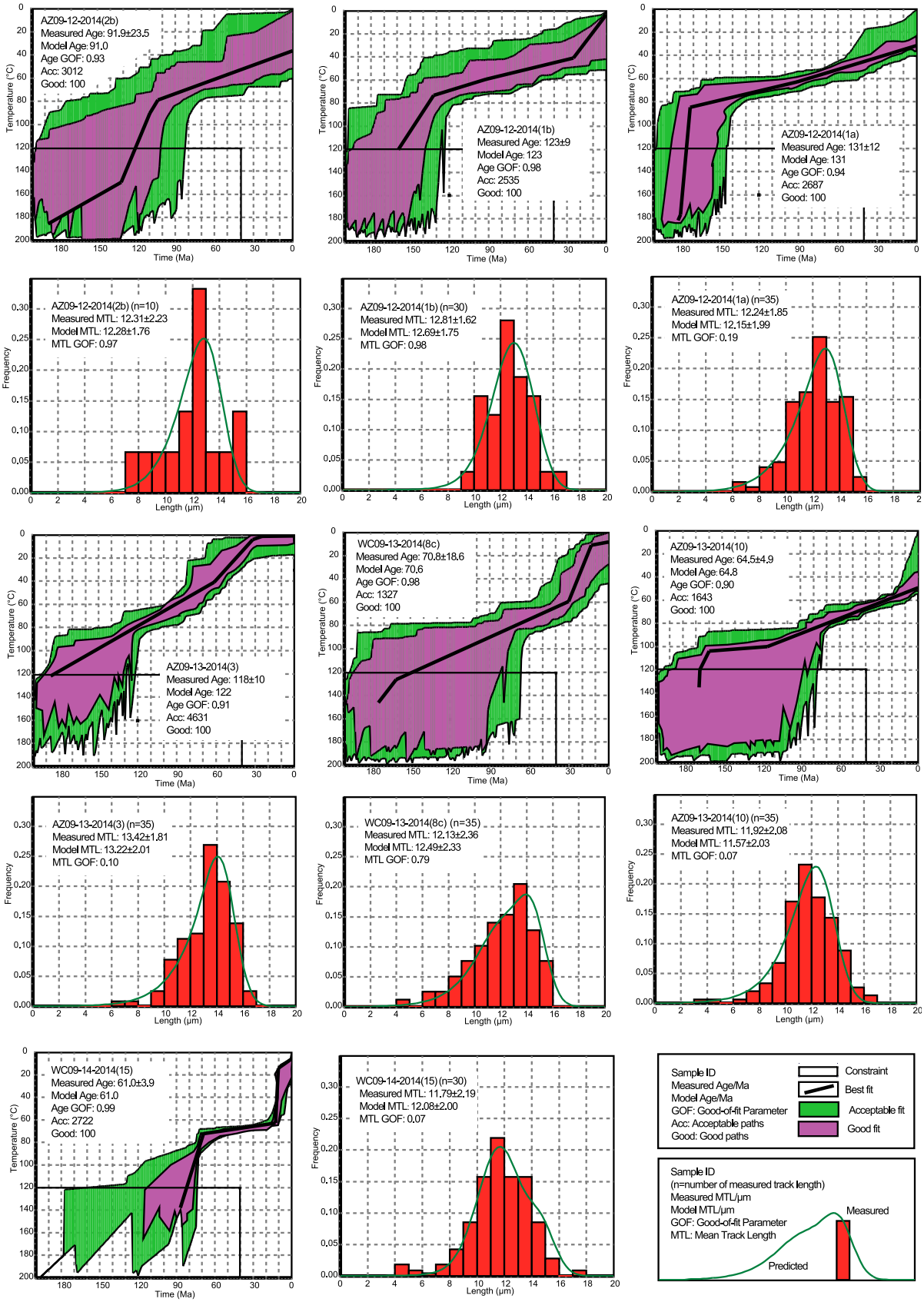

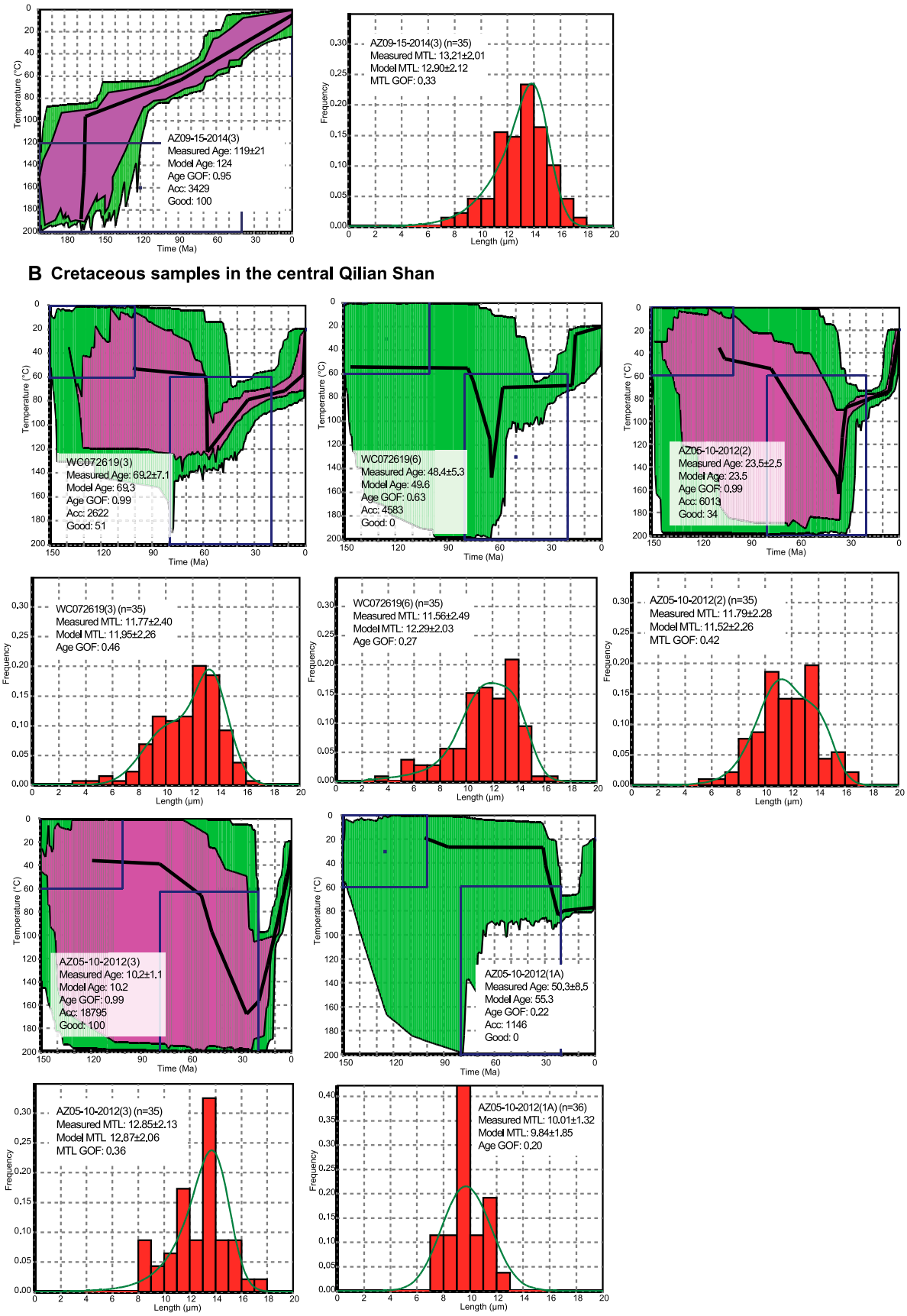

Figure 8. (continued)

C Proterozoic-Paleozoic samples in the Longshou Shan

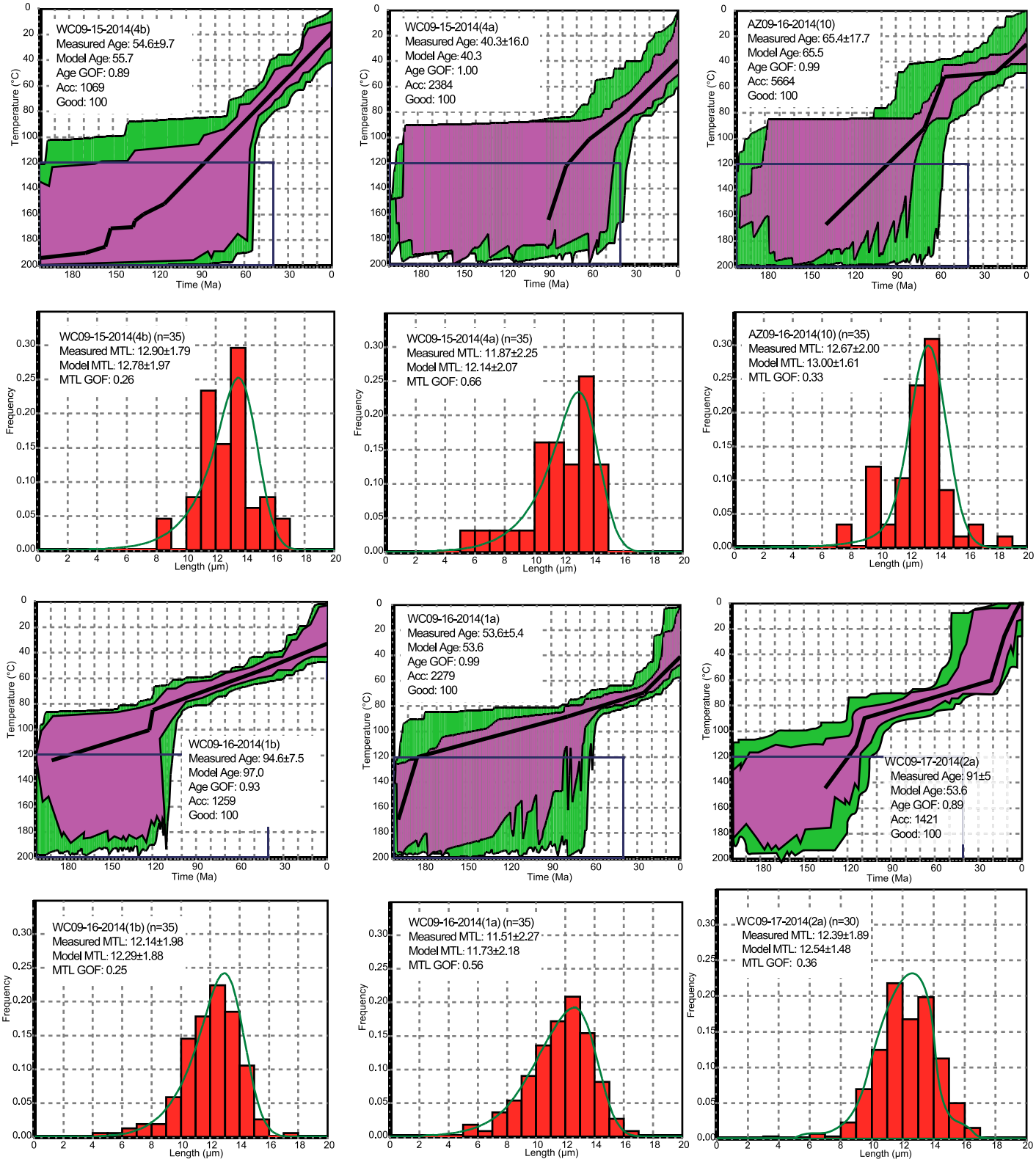

Figure 8. (continued)

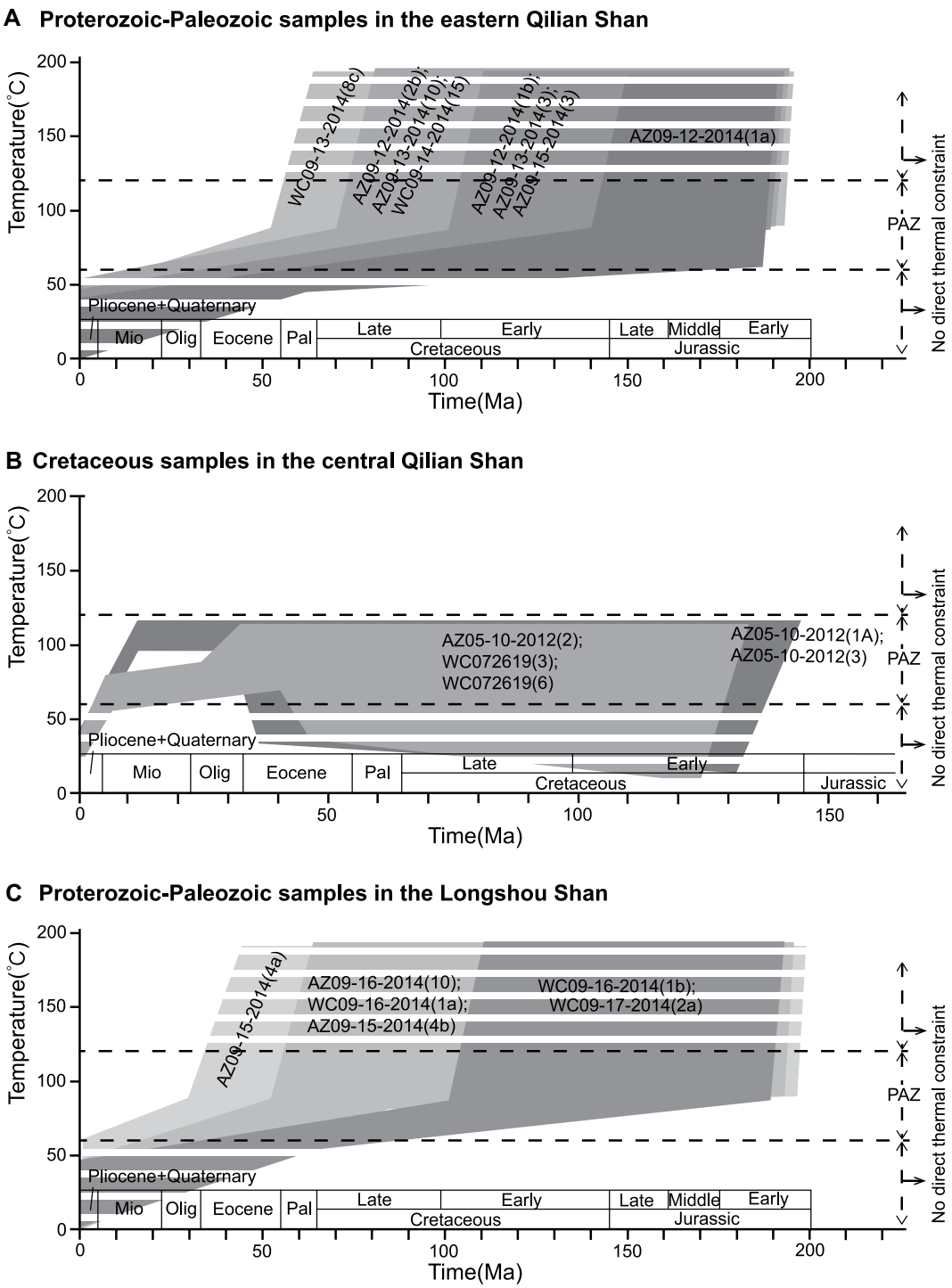

Figure 9. (A) Summary provides thermal history modeling results of Proterozoic–Paleozoic samples across the eastern Qilian Shan with good paths reported in this study. (B) Summary of thermal history modeling results of Cretaceous samples in the central Qilian Shan with good paths reported in this study. (C) Summary of thermal history modeling results of Proterozoic–Paleozoic samples across the Longshou Shan with good paths reported in this study.

with the low-temperature thermochronology data sets across northern Tibet and the regional unconformity across the northern plateau (e.g., Wu et al., 2011; Zuza et al., 2018). In addition, Chen et al. (2019a) reported a contractional deformation system including a strike-slip duplex, thrust nappe, and klippe structure in the northeastern Qilian Shan, which suggests a regional tectonic uplift event. We interpret that this exhumation event may be driven by the far-field response to the closure of the Paleo-Tethys and Meso-Tethys Oceans and the collision between the Lhasa and Eurasia continents from the Triassic to possibly the earliest Jurassic (e.g., Pullen et al., 2008; Zhang et al., 2014; Wu et al., 2016, 2017, 2019b; Kapp et al., 2007; Li et al., 2017b; Kapp and DeCelles, 2019; Jolivet et al., 2015) and the far-field effects on the late Mesozoic Hexi Corridor. The Cretaceous cooling history is also widely observed in our AFT grain age distribution results (Figs. 8A and 9A).

The discrete period of rapid cooling during and since the Eocene is likely related to the far-field effects of the India–Asia collision (e.g., An et al., 2020; Li et al., 2019, 2020; He et al., 2020). Previous AFT ages and thermal history modeling results suggested a rapid cooling of

the South Qilian Shan and the northern margin of the Qaidam basin, which resulted from fault-related uplift and exhumation of south-central Qilian Shan thrusts at ca. 50–40 Ma (e.g., Jolivet et al., 2001; Clark et al., 2010; Zuza et al., 2016; Li et al., 2019, 2020). Furthermore, the northern Altyn Tagh Range, northwestern Eastern Kunlun Range, and the western end of the Qinling region also exhibit the rapid cooling event in this period (e.g., Clark et al., 2010; Duvall et al., 2011; Jolivet et al., 2001; Yin et al., 2002; Ritts et al., 2008; Mock et al., 1999; Wang and Burchfiel, 2004). Evidence from regional geologic studies supports the early Cenozoic tectonic exhumation event in the Qilian Shan and includes the deposition of coarse clastic deposits unconformably overlying Cretaceous sedimentary rocks in the northern Qaidam Basin (e.g., Ji et al., 2017; Zhuang et al., 2011; Wu et al., 2019b; He et al., 2020) and coarse clast-dominated sediment that rapidly accumulated over the Cretaceous in the Xining Basin during the early Eocene (Fang et al., 2019).

The deformation of the Northern Qilian Shan thrusts started at ca. 30–25 Ma, which is consistent with a regional unconformable contact between the Huoshaogou Formation and overlying Baiyanghe Formation in the Qilian Shan and Hexi Corridor areas (i.e., Lin et al., 2011; Li et al., 2019, 2020; An et al., 2020). Our thermal history modeling results from eastern Qilian Shan samples clearly show the stage of cooling event in this period (Figs. 8 and 9A). That is, the northeastward growth of the plateau in the Qilian Shan was accommodated by slip along a series of thrust faults. The cooling event since the middle Miocene has been recorded by Paleozoic granite sample AZ 09-14-2014 (15), which may correspond to the reactivation of the Northern Qilian Shan thrust belt and the initiation of the western segment of the Haiyuan fault (e.g., George et al., 2001; Zheng et al., 2010, 2017; Lin et al., 2011; Wang et al., 2011; Lease et al., 2012; Yuan et al., 2013; Zhuang et al., 2018; Li et al., 2019, 2020; Yu et al., 2019a, 2019b; Chen et al., 2019b; Wang et al., 2020a) (Figs. 8A and 9A).

Thermal and Tectonic History Inferred from the Cretaceous Samples

The AFT results from the Cretaceous sandstone samples suggest that following Cretaceous deposition, the samples were reheated to ~80–100 °C, probably via burial, and then cooled again (Fig. 9B). We interpret that the samples were not reheated by simple sedimentary burial because the thickness of Cretaceous strata in the Qilian Shan (i.e., ≤1.4 km; Qinghai BGMR, 1991; Pan et al., 2004; Zuza et al., 2018) is not enough to heat the samples to AFT PAZ conditions. Therefore, we posit that most of the Cretaceous samples were tectonically buried via thrusting in the Mesozoic or early Cenozoic. The track length distributions for these samples have wide and low amplitude, consistent with reheating and/or long residence within the AFT PAZ (Table 1; e.g., Gleadow et al., 1986; Green, 1988), which is consistent with our model for thrust-related burial of these samples (Fig. 10). Cretaceous strata are commonly observed in fault contact with older units (i.e., Ordovician or Carboniferous strata) (e.g., Zuza et al., 2018, 2019; Chen et al., 2019a; Li et al., 2020; Figs. 4D–4F). Zuza et al. (2019) documented a large thrust fault, where Ordovician rocks were juxtaposed over Cretaceous strata (Fig. 8A in Zuza et al., 2019). The AFT thermal histories suggest that these samples were exhumed from AFT PAZ depths in the Miocene.

Field relationships in this study show Ordovician and Carboniferous rocks in thrust contact with Cretaceous strata (Figs. 4D–4F), which is consistent with the AFT-derived thermal histories. Cretaceous sedimentary rocks were first deposited over upper Paleozoic strata (Fig. 10). Sometime in the late Mesozoic to early Cenozoic, a package of Carboniferous and younger rocks was thrust over the Cretaceous strata, which buried the apatite samples analyzed to AFT PAZ depths (Figs. 4D and 10). Later, potentially related to the initiation of left-lateral transpression associated with the Haiyuan fault (i.e., Li et al., 2019), renewed thrusting and uplift juxtaposed Ordovician rocks with the Carboniferous and Cretaceous strata and led to exhumation of these rocks, as is recorded in the AFT systematics (Figs. 4D and 10). Northward tilting of the Cretaceous strata by north-directed thrusting could have occurred during any of these events (Figs. 4D and 10).

Alternative mechanisms to reheat the Cretaceous samples include: (1) internal burial via intra-Cretaceous strata repetition rather than the coherent thrust sheet discussed above, (2) enhanced burial by additional early Cenozoic sediments, or (3) reheating by proximal intrusions or fluids. We argue that the first mechanism is similar to our proposed model (Fig. 10) with respect to the broader interpretations, such that early Cenozoic shortening affected the study area. Known early Cenozoic sediments are sparse and relatively thin in the central Qilian Shan, which suggests that they could not have significantly buried and heated these samples (Qinghai BGMR, 1991; Pan et al., 2004; Fang et al., 2019). If some unknown early Cenozoic sediments did bury Cretaceous rocks enough to reheat them, and have since eroded, the only plausible geologic events to source such thick sediments during this time would be contraction-related uplift. This would imply early Cenozoic deformation similar to our preferred interpretation. Lastly, there are no known or reported Cenozoic volcanic rocks or intrusions in the Qilian Shan to have heated the samples. It is also

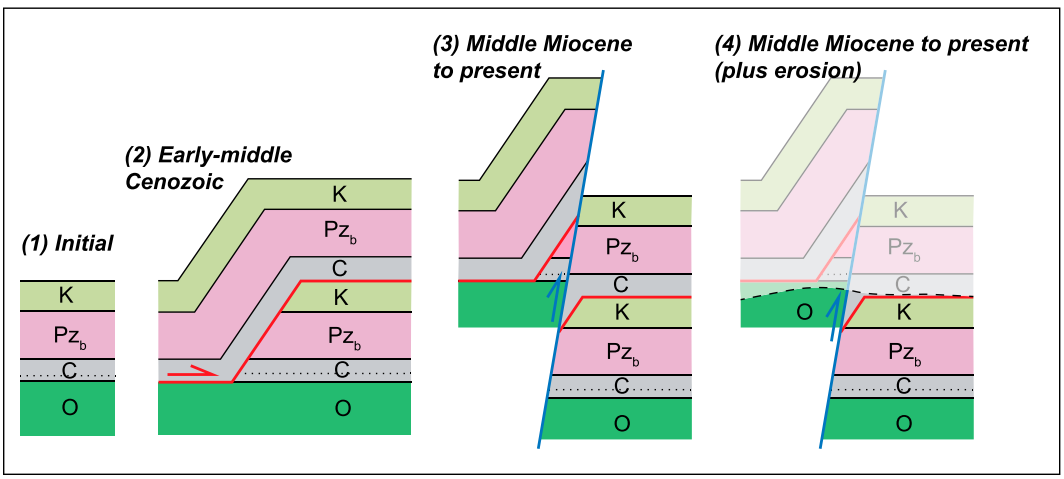

Figure 10. A simple model summarizes the deformation history of the Cenozoic Qilian Shan thrust.

unlikely that these intrusions would only have affected AFT analyses of Cretaceous sediments (Li et al., 2020; this study). However, heating by fluid flow through the high permeability sandstones is possible and perhaps could have been enhanced by nearby faults and fracture-related permeability. We did not observe alteration or silicification near the samples studied, and therefore our observations do not independently support this model. All three of these alternative scenarios may suggest some early Cenozoic tectonic activity.

Thermal and Tectonic History of the Longshou Shan in the Qilian Shan Foreland

The thermal models of our Longshou Shan samples suggest that three significant cooling events took place since the Early–Middle Jurassic, during/since the Late Cretaceous, and since the Miocene (Figs. 8C and 9C). The cooling event since the Early–Middle Jurassic observed in the eastern Longshou Shan samples may been associated with far-field effects of the closure of the Paleo-Tethys and Meso-Tethys Oceans in the south (e.g., Pullen et al., 2008; Zhang et al., 2014; Wu et al., 2016, 2017, 2019b), the collision between the Lhasa and Qiangtang continents at ca. 200–150 Ma (Kapp et al., 2007; Li et al., 2017b; Kapp and DeCelles, 2019), and/or the possible latest Jurassic–earliest Cretaceous closure of the Mongolia-Okhotsk ocean in the north between the North China and Siberian cratons (e.g., Cogné et al., 2005; Van der Voo et al., 2015; Jolivet et al., 2015). Our Longshou Shan AFT samples are located at the hanging wall of the Longshou Shan thrust (Figs. 2B and 5E), which would have been active along the southwestern margin of the North China craton. In addition, Feng et al. (2017) reported the late Mesozoic fault activity in the western margin of the North China craton from a multi-chronometer study involving apatite helium, apatite fission track, and $^{40}Ar/^{39}Ar$ thermochronology. A Late Cretaceous rapid cooling event is rarely reported in the western margin of the North China craton, which possibly suggests that this was a relatively local exhumation event. Although this deformational process is not well contained, the exhumation event is consistent with the absence of the upper Cretaceous strata in the Longshou Shan region (e.g., Gansu BGMR, 1969; Vincent and Allen, 1999; Pan et al., 2004).

After relative tectonic quiescence during the early Cenozoic in the Longshou Shan area, rapid cooling since the Miocene demonstrates the far-field effects of intracontinental growth and tectonic deformation on the northeastern margin of the plateau with reactivation of the Longshou Shan thrust (e.g., Duvall et al., 2013; Yuan et al., 2013; Zuza and Yin, 2016; Feng et al., 2017; Song et al., 2018; Li et al., 2019, 2020). In addition, Zheng et al. (2013) reported a ca. 2 Ma thrusting event along the southern margin of the Heli Shan northwest of Longshou Shan, which should be reactivation rather than the rapid uplift caused by initial thrusting.

Tectonic History

Our thermochronological results imply that the northeastern Tibetan Plateau and foreland region underwent regional late Mesozoic exhumation, including the western margin of the North China craton. From our traverse, samples collected above 2500 m elevation yield a range of AFT ages from ca. 68 Ma to ca. 131 Ma (Table 1) and thus were at PAZ temperatures for most of the late Mesozoic (Fig. 9). These analyses suggest that the eastern Qilian Shan–Longshou Shan were not significantly deforming or exhuming prior to the Cretaceous–early Cenozoic.

Although the deformation mechanism for late Mesozoic exhumation is not well constrained, the regional event is generally interpreted to be associated with the consumption of the Paleo-Tethys and Meso-Tethys Oceans south of the Qilian-Qaidam-Kunlun continent from the Triassic to possibly the earliest Jurassic (Fig. 1). An additional possible effect on the Longshou Shan area is the Latest Jurassic–earliest Cretaceous closure of the Mongolia-Okhotsk Ocean north of the North China craton. Late Cretaceous exhumation is widespread in the northern Tibetan Plateau (e.g., George et al., 2001; Jolivet et al., 2001; An et al., 2020; Tian et al., 2020; Li et al., 2019, 2020), and the scattered, synchronous, coarse-grain, clastic molasse strata were deposited in the Hexi Corridor (e.g., Liu et al., 2001; Vincent and Allen, 1999). This tectonic event is also shown in our AFT thermal modeling results from the hanging wall of the Longshou Shan thrust, i.e., the southwestern margin of the North China Craton.

Of note, this pronounced, pre-Cenozoic cooling signal implies deformation-related exhumation of northern Tibet prior to the India-Asia collision (e.g., Jolivet et al., 2001; Chen et al., 2019b). The extent and magnitude of late Mesozoic deformation remains poorly resolved, but models of plateau growth and intracontinental strain in the Himalayan-Tibetan orogen rarely consider this phase of deformation. Cenozoic structures may have reactivated earlier faults, which makes teasing out this phase of deformation more problematic. However, recent studies arguing that the Qaidam Basin was at or near sea level in the earliest Cenozoic (e.g., Kaya et al., 2019) imply that pre-Cenozoic shortening in northern Tibet was a relatively minor event that did not significantly elevate topography.

Models for Cenozoic deformation in the Qilian Shan as part of the Himalayan-Tibetan orogen can be grouped into northward-propagating deformation or early out-of-sequence shortening. The northward-propagating deformation models predict the oldest deformation in the Fenghoushan and Eastern Kunlun Range thrust systems to the south, which is followed by more recently initiated deformation in the Qilian Shan as the orogen propagates in-sequence northward (e.g., Pang et al., 2019; Yu et al., 2019b; Zheng et al., 2010, 2017; Zhuang et al., 2018; Wang et al., 2020a). Alternatively, deformation occurred shortly after India-Asia collision in the Qilian Shan, thus defining the northern boundary of the Himalayan-Tibetan orogen early in the Cenozoic (e.g., Clark, 2012), and subsequent shortening has occurred within the orogen's interior.

Cooling recorded by our AFT observations suggests that early Cenozoic deformation of the Qilian Shan initiated in the Eocene, which accommodated far-field compressional stress transmitted from the early Cenozoic India-Asia collision along the pre-existing tectonic sutures (Fig. 1) (e.g., Zuza et al., 2019; Bian et al., 2020; Chen et al., 2020). Early deformation along the northernmost margin of the plateau, overprinted by later Miocene-to-present deformation, argues for out-of-sequence thrusting rather than progressive, northward-propagating deformation (Figs. 11A and 11B). The regional unconformity between the Eocene deposits and the lower Cretaceous strata is developed in the Jiuxi basin, which indicates the presence of the Late Cretaceous–Paleogene tectonic activity (i.e., An et al., 2020). Independent support for early Cenozoic deformation initiation comes from the deformation record observed across the Qilian Shan. Estimates of minimum Cenozoic shortening across the Qilian Shan are ~300–350 km, which is consistent with required crustal thickening from average crustal thickness values of ~35 km. This is consistent with near sea level elevations in the earliest Cenozoic to ~60 km+ today (Zuza et al., 2016, 2018; Cheng et al., 2015). A Miocene initiation of shortening in the Qilian Shan (e.g., Pang et al., 2019; Yu et al., 2019a; Zheng et al., 2010, 2017; Zhuang et al., 2018; Wang et al., 2020a) implies bulk average shortening rates of >20 mm/yr, which is almost four times the present day convergence rate (~5–6 mm/yr) across the region (e.g., Zhang et al., 2004). Conversely, an Eocene initiation age equates to average shortening rates of ~8 mm/yr, which is slightly higher than the present-day rates (e.g.,

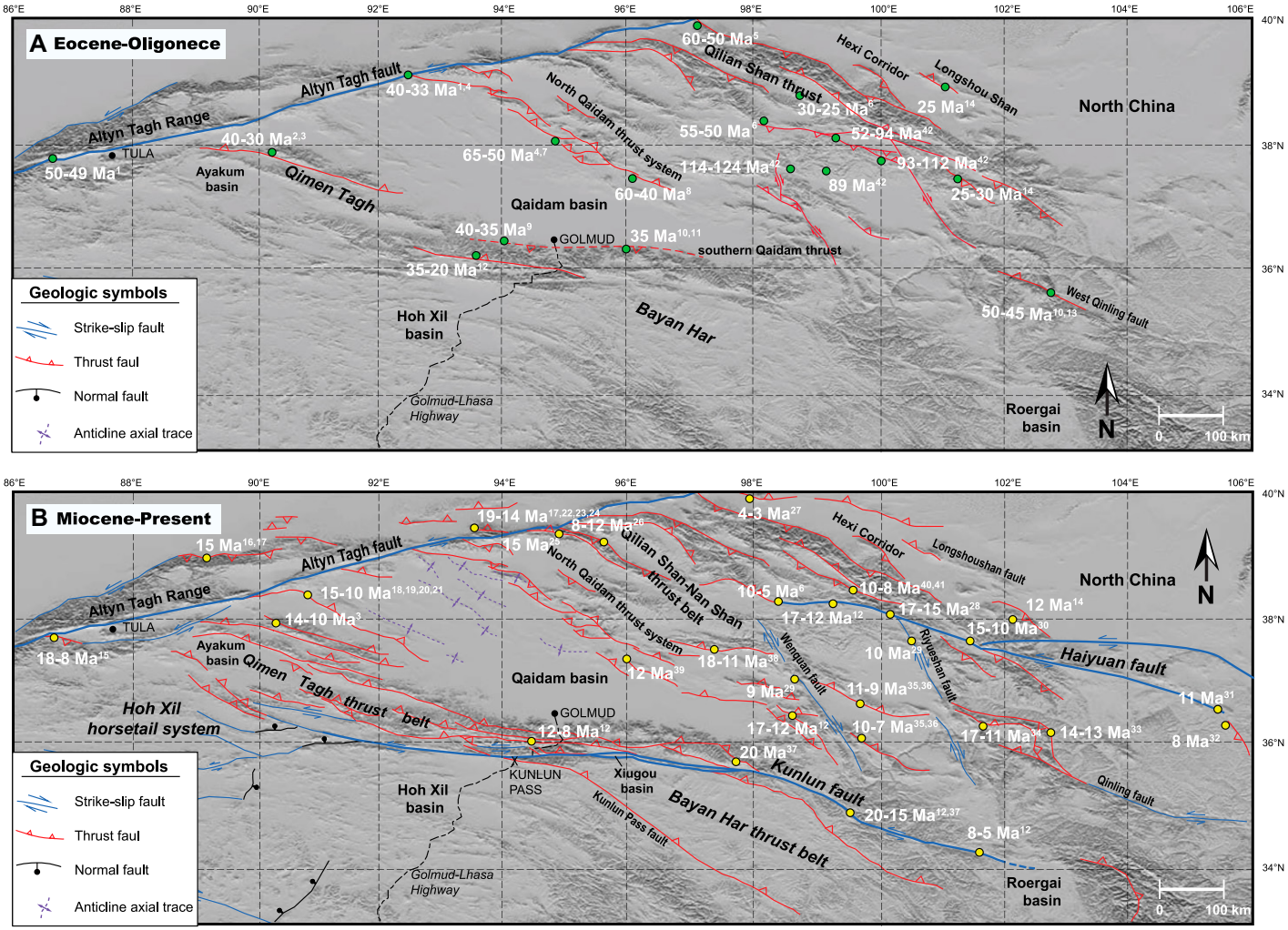

Figure 11. (A) Eocene–Oligocene fault deformation in the northeastern margin of the Tibetan Plateau and Hexi Corridor is shown. (B) Miocene–present deformation in the northeastern margin of the Tibetan Plateau, Hexi Corridor, and Longshou Shan. The thermochronology data are shown in Table S1 (see footnote 1). Data are from: 1—Yin et al. (2002); 2—D. Liu et al. (2017a); 3—Y. Wang et al. (2018); 4—Jolivet et al. (2001); 5—He et al. (2017); 6—Li et al. (2020); 7—Yin et al. (2008a); 8—He et al. (2018); 9—F. Wang et al. (2017a); 10—Clark et al. (2010); 11—Mock et al. (1999); 12—Duvall et al. (2013); 13—Duvall et al. (2011); 14—this study; 15—Wu et al. (2020); 16—Ritts et al. (2008); 17—Shi et al. (2018); 18—F. Cheng et al. (2015); 19—R. Liu et al. (2017b); 20—Chang et al. (2015); 21—Li et al. (2017a); 22—X. Wang et al. (2003); 23—Sun et al. (2005); 24—Lin et al. (2015); 25—J. Yu et al. (2019a); 26—Zhuang et al. (2018); 27—Palumbo et al. (2010); 28—Yu et al. (2017); 29—Yuan et al. (2011); 30—Li et al. (2019); 31—W. Wang et al. (2011); 32—Zheng et al. (2006); 33—Lease et al. (2011); 34—Yan et al. (2006); 35—Craddock et al. (2011); 36—Craddock et al. (2014); 37—Yuan et al. (2006b); 38—Pang et al. (2019); 39—W. Wang et al. (2017b); 40—Zheng et al. (2010); 41—Zheng et al. (2017); 42—B. Qi et al. (2016).

Zuza et al., 2020) and consistent with faster India-Asia convergence rates in the early Cenozoic (e.g., Copley et al., 2010).

Cenozoic deformation and uplift of the Hexi Corridor and Longshou Shan regions north of the Qilian Shan initiated in the Miocene (Figs. 9 and 10). The widespread tectonic deformation along the northeastern Tibetan Plateau and Hexi Corridor-Longshou Shan since the Miocene suggests significant outward intracontinental growth of the plateau and basin-range evolution with the reactivation of thrusts and initiation of the Haiyuan transpressional fault system (Fig. 11B). We suggest that the Miocene activities of the Northern Qilian Shan thrusts and Longshou Shan thrust represent a reactivation event rather than initiation, and more than half of the Cenozoic shortening and crustal thickening across the northern plateau may have occurred prior to the Miocene (e.g., Zuza et al., 2019, 2020; Li et al., 2020) (Figs. 11A and 11B). Furthermore, Miocene to present intracontinental growth and deformation of the northern Tibetan Plateau are mainly controlled by the Altyn Tagh strike-slip fault and the Kunlun and Haiyuan transpressional fault systems (Fig. 11B).

CONCLUSIONS

Field observations, AFT analysis, and thermal history modeling provide constraints on the complex exhumation history from the late Mesozoic to Cenozoic in the eastern Qilian Shan, central Qilian Shan, and Longshou Shan regions of northern Tibet. The spatiotemporal cooling patterns established by this study require the multi-phase intracontinental growth history of the northern Tibetan Plateau and its foreland region. The regional late Mesozoic exhumation event recorded across the northern plateau is in-

terpreted to be associated with the consumption of the Paleo-Tethys and Meso-Tethys Oceans south of the Qilian-Qaidam-Kunlun continent from the Triassic to the earliest Jurassic. Another driver for the Mesozoic cooling event recorded in northern Tibet and its foreland region is the latest Jurassic–earliest Cretaceous closure of the Mongolia-Okhotsk Ocean that defines the northern margin of the North China craton. The Late Cretaceous cooling data are best explained by a regional extensional event as reported by earlier studies. Thrusting in the Qilian Shan may have initiated in the Eocene as suggested by our thermochronological data, which support out-of-sequence rather than northward-migrating plateau growth. The early Cenozoic structural pattern was reorganized in the middle Miocene, which is associated with the initiation of the Haiyuan left-slip fault system and its compressional and extensional termination structures. Cenozoic deformation and uplift of the Hexi Corridor and Longshou Shan region directly north of the Qilian Shan started in the Miocene and resulted from outward growth of the plateau.

ACKNOWLEDGMENTS

We thank Editor Rob Strachan, Associate Editor Tim Kusky, Kai Cao, and one anonymous reviewer for their critical, careful, and very constructive reviews that helped to improve the clarity and interpretations of the original draft. This research was supported by grants from the Basic Science Center for Tibetan Plateau Earth System (CTPES, 41988101-01), the Second Tibetan Plateau Scientific Expedition and Research Program (2019QZKK0708), National Natural Science Foundation of China (41702232, 41941016, and 41661134049), the National Key Research and Development Project of China (2016YFC0600303), the Chinese Academy of Sciences, Strategic Priority Research Program (XDA20070301), the China Geological Survey (DD20160083), and the NSF Tectonics program of the National Science Foundation (EAR 1914501).

REFERENCES CITED

Allen, M.B., Walters, R.J., Song, S., Saville, C., De Paola, N., and Ford, J., 2017, Partitioning of oblique convergence coupled to the fault locking behavior of fold-and-thrust belts: Evidence from the Qilian Shan, northeastern Tibetan Plateau: Tectonics, v. 36, p. 1679–1698, https://doi.org/10.1002/2017TC004476.

An, K., Lin, X., Wu, L., Yang, R., Chen, H., Cheng, X., Xia, Q., Zheng, F., Ding, W., Gao, S., Li, C., and Zhang, Y., 2020, An immediate response to the Indian-Eurasian collision along the northeastern Tibetan Plateau: Evidence from apatite fission track analysis in the Kuantan Shan-Hei Shan: Tectonophysics, v. 774, p. 228–278, https://doi.org/10.1016/j.tecto.2019.228278.

Bai, J., and Dai, F.Y., 1996, The early Precambrian crustal evolution of China [in Chinese with English Abstract]: Journal of Southeast Asian Earth Sciences, v. 13, no. 3–5, p. 205–214.

Bian, S., Gong, J., Chen, L., Zuza, A.V., Chen, H., Lin, X., Cheng, X.G., and Yang, R., 2020, Diachronous uplift in intra-continental orogeny: 2D thermo-mechanical modeling of the India-Asia collision: Tectonophysics, v. 775, p. 228310, https://doi.org/10.1016/j.tecto.2019.228310.

Burchfiel, B.C., Zhang, P., Wang, Y., Zhang, W., Song, F., Deng, Q., Molnar, P., and Royden, L., 1991, Geology of the Haiyuan fault zone, Ningxia-Hui Autonomous Region, China, and its relation to the evolution of the northeastern margin of the Tibetan Plateau: Tectonics, v. 10, no. 6, p. 1091–1110, https://doi.org/10.1029/90TC02685.

Burchfiel, C.B., and Royden, L.H., 1991, Tectonics of Asia 50 years after the death of Emile Argand: Eclogae Geologicae Helvetiae, v. 84, no. 3, p. 599–629.

Cao, K., Wang, G.C., van der Beek, P., Bernet, M., and Zhang, K.X., 2013, Cenozoic thermo-tectonic evolution of the northeastern Pamir revealed by zircon and apatite fission-track thermochronology: Tectonophysics, v. 589, p. 17–32, https://doi.org/10.1016/j.tecto.2012.12.038.

Cao, K., Wang, G.C., Bernet, M., van der Beek, P., and Zhang, K.X., 2015, Exhumation history of the West Kunlun Mountains, northwestern Tibet: Evidence for a long-lived, rejuvenated orogen: Earth and Planetary Science Letters, v. 432, p. 391–403, https://doi.org/10.1016/j.epsl.2015.10.033.

Cao, K., Leloup, P.H., Wang, G.C., Liu, W., Mahéo, G., Shen, T.Y., Xu, Y.D., Sorrel, P., and Zhang, K.X., 2021, Thrusting, exhumation, and basin fill on the western margin of the South China block during the India-Asia collision: Geological Society of America Bulletin, v. 133, no. 1–2, p. 74–90, https://doi.org/10.1130/B35349.1.

Chang, H., Li, L., Qiang, X., Garzione, C.N., Pullen, A., and An, Z., 2015, Magnetostratigraphy of Cenozoic deposits in the western Qaidam Basin and its implication for the surface uplift of the northeastern margin of the Tibetan Plateau: Earth and Planetary Science Letters, v. 430, p. 271–283, https://doi.org/10.1016/j.epsl.2015.08.029.

Chen, L., Liu, L., Capitanio, F.A., Gerya, T.V., and Li, Y., 2020, The role of pre-existing weak zones in the formation of the Himalaya and Tibetan plateau: 3-D thermomechanical modelling: Geophysical Journal International, v. 221, no. 3, p. 1971–1983, https://doi.org/10.1093/gji/ggaa125.

Chen, X.H., Yin, A., Gehrels, G.E., Cowgill, E.S., Grove, M., Harrison, T.M., and Wang, X.F., 2003, Two phases of Mesozoic north-south extension in the eastern Altyn Tagh range, northern Tibetan Plateau: Tectonics, v. 22, no. 5, https://doi.org/10.1029/2001TC001336.

Chen, X.H., Shao, Z., Xiong, X., Gao, R., Xu, S., Zhang, Y., Li, B., and Wang, Y., 2019a, Early Cretaceous overthrusting of Yumu mountain and hydrocarbon prospect on the Northern margin of the Qilian orogenic belt [in Chinese with English abstract]: Acta Geoscientica Sinica, v. 40. no. 3, p. 377–392, https://doi.org/10.3975/cagsb.2019.050901.

Chen, X.H., Shao, Z., Xiong, X., Gao, R., Liu, X., Wang, C., Li, B., Wang, Z., and Zhang, Y., 2019b, Fault system, deep structure and tectonic evolution of the Qilian Orogenic Belt, Northwest China [in Chinese with English abstract]: Geology in China, v. 46, no. 5, p. 995–1020, https://doi.org/10.12029/gc20190504.

Cheng, F., Guo, Z., Jenkins, H.S., Fu, S., and Cheng, X., 2015, Initial rupture and displacement on the Altyn Tagh fault, northern Tibetan Plateau: Constraints based on residual Mesozoic to Cenozoic strata in the western Qaidam Basin: Geosphere, v. 11, no. 3, p. 921–942, https://doi.org/10.1130/GES01070.1.

Cheng, F., Garzione, C.N., Jolivet, M., Guo, Z., Zhang, D., Zhang, C., and Zhang, Q., 2019, Initial deformation of the northern Tibetan plateau: Insights from deposition of the Lulehe Formation in the Qaidam Basin: Tectonics, v. 38, no. 2, p. 741–766, https://doi.org/10.1029/2018TC005214.

Clark, M.K., 2012, Continental collision slowing due to viscous mantle lithosphere rather than topography: Nature, v. 483, no. 7387, p. 74, https://doi.org/10.1038/nature10848.

Clark, M.K., Farley, K.A., Zheng, D., Wang, Z., and Duvall, A.R., 2010, Early Cenozoic faulting of the northern Tibetan Plateau margin from apatite (U-Th)/He ages: Earth and Planetary Science Letters, v. 296, no. 1–2, p. 78–88, https://doi.org/10.1016/j.epsl.2010.04.051.

Cogné, J.-P., Kravchinsky, V.A., Halim, N., and Hankard, F., 2005, Late Jurassic-Early Cretaceous closure of the Mongol-Okhotsk Ocean demonstrated by new Mesozoic palaeomagnetic results from the Trans-Baikal area (SE Siberia): Geophysical Journal International, v. 163, p. 813–832, https://doi.org/10.1111/j.1365-246X.2005.02782.x.

Copley, A., Avouac, J.P., and Royer, J.Y., 2010, India-Asia collision and the Cenozoic slowdown of the Indian plate: Implications for the forces driving plate motions: Journal of Geophysical Research: Solid Earth, v. 115, B3, no. B03410, https://doi.org/10.1029/2009JB006634.

Craddock, W., Kirby, E., and Zhang, H., 2011, Late Miocene–Pliocene range growth in the interior of the northeastern Tibetan Plateau: Lithosphere, v. 3, no. 6, p. 420–438, https://doi.org/10.1130/L159.1.

Craddock, W.H., Kirby, E., Zhang, H., Clark, M.K., Champagnac, J.D., and Yuan, D., 2014, Rates and style of Cenozoic deformation around the Gonghe Basin, northeastern Tibetan Plateau: Geosphere, v. 10, no. 6, p. 1255–1282, https://doi.org/10.1130/GES01024.1.

Dai, S., Fang, X., Dupont-Nivet, G., Song, C., Gao, J., and Krijgsman, W., et al., 2006, Magnetostratigraphy of Cenozoic sediments from the Xining Basin: Tectonic implications for the northeastern Tibetan Plateau: Journal of Geophysical Research: Solid Earth, v. 111, no. B11102, https://doi.org/10.1029/2005JB004187.

Donelick, R.A., and Miller, D.S., 1991, Enhanced TINT fission track density apatites using ^{252}Cf-derived fission fragment tracks: A model and experimental observations: Nuclear Tracks and Radiation Measurements, v. 18, p. 301–307, https://doi.org/10.1016/1359-0189(91)90022-A.

Donelick, R.A., O'Sullivan, P.B., and Ketcham, R.A., 2005, Apatite fission-track analysis: Reviews in Mineralogy and Geochemistry, v. 58, p. 49–94, https://doi.org/10.2138/rmg.2005.58.3.

Dupont-Nivet, G., Horton, B.K., Butler, R.F., Wang, J., Zhou, J., and Waanders, G.L., 2004, Paleogene clockwise tectonic rotation of the Xining-Lanzhou region, northeastern Tibetan Plateau: Journal of Geophysical Research: Solid Earth, v. 109, no. B04401, https://doi.org/10.1029/2003JB002620.

Duvall, A.R., Clark, M.K., van der Pluijm, B.A., and Li, C., 2011, Direct dating of Eocene reverse faulting in northeastern Tibet using Ar-dating of fault clays and low-temperature thermochronometry: Earth and Planetary Science Letters, v. 304, no. 3–4, p. 520–526, https://doi.org/10.1016/j.epsl.2011.02.028.

Duvall, A.R., Clark, M.K., Kirby, E., Farley, K.A., Craddock, W.H., Li, C., and Yuan, D.Y., 2013, Low-temperature thermochronometry along the Kunlun and Haiyuan Faults, NE Tibetan Plateau: Evidence for kinematic change during late-stage orogenesis: Tectonics, v. 32, no. 5, p. 1190–1211, https://doi.org/10.1002/tect.20072.

England, P., and Houseman, G., 1986, Finite strain calculations of continental deformation: 2. Comparison with the India-Asia collision zone: Journal of Geophysical Research, v. 91, no. B3, p. 3664–3676, https://doi.org/10.1029/JB091iB03p03664.

Fan, S.Y., and Murphy, M.A., 2021, Three-dimensional strain accumulation and partitioning in an arcuate orogenic wedge: An example from the Himalaya: Geological Society of America Bulletin, v. 133, no. 1–2, p. 3–18, https://doi.org/10.1130/B35528.1.

Fang, X., Liu, D., Song, C., Dai, S., and Meng, Q., 2013, Oligocene slow and Miocene–quaternary rapid deformation and uplift of the Yumu Shan and north Qilian Shan: Evidence from high-resolution magnetostratigraphy and tectonosedimentology, *in* Jovane, L., Herrero-Bervera, E., Hinnov, L.A., and Housen, B., eds., Magnetic Methods and the Timing of Geological Processes: Geological Society, London, Special Publication 373, no. 1, p. 149–171, https://doi.org/10.1144/SP373.5.

Fang, X.M., Fang, Y.H., Zan, J.B., Zhang, W.L., Song, C.H., Appel, E., Meng, Q.Q., Miao, Y.F., Dai, S., Li, Y., and Zhang, T., 2019, Cenozoic magnetostratigraphy of the Xining Basin, NE Tibetan Plateau, and its constraints on paleontological, sedimentological and tectonomorphological evolution: Earth-Science Reviews, v. 190, p. 460–485, https://doi.org/10.1016/j.earscirev.2019.01.021.

Feng, L.X., Brown, R.W., Han, B.-F., Wang, Z.-Z., Łuszczak, K., Liu, B., Zhang, Z.-C., and Ji, J.-Q., 2017, Thrusting and exhumation of the southern Mongolian Plateau: Joint thermochronological constraints from the

Langshan Mountains, western Inner Mongolia, China: Journal of Asian Earth Sciences, v. 144, p. 287–302, https://doi.org/10.1016/j.jseaes.2017.01.001.

Flowers, R.M., Farley, K.A., and Ketcham, R.A., 2015, A reporting protocol for thermochronologic modeling illustrated with data from the Grand Canyon: Earth and Planetary Science Letters, v. 432, p. 425–435, https://doi.org/10.1016/j.epsl.2015.09.053.

Galbraith, R.F., and Green, P.F., 1990, Estimating the component ages in a finite mixture: International Journal of Radiation Applications and Instrumentation. Part D: Nuclear Tracks and Radiation Measurements, v. 17, no. 3, p. 197–206, https://doi.org/10.1016/1359-0189(90)90035-V.

Galbraith, R.F., and Laslett, G.M., 1993, Statistical models for mixed fission track ages: Nuclear Tracks and Radiation Measurements, v. 21, p. 459–470, https://doi.org/10.1016/1359-0189(93)90185-C.

Gallagher, K., Brown, R., and Johnson, C., 1998, Fission track analysis and its applications to geological problems: Annual Review of Earth and Planetary Sciences, v. 26, p. 519–572, https://doi.org/10.1146/annurev.earth.26.1.519.

Gansu Bureau of Geology and Mineral Resources (BGMR), 1969, Geologic map of the Baoensi [in Chinese]: Geological House, Beijing, scale 1: 200,000.

Gao, R., Wang, H., Yin, A., Dong, S., Kuang, Z., Zuza, A.V., Li, W., and Xiong, X., 2013, Tectonic development of the northeastern Tibetan Plateau as constrained by high-resolution deep seismic-reflection data: Lithosphere, v. 5, no. 6, p. 555–574, https://doi.org/10.1130/L293.1.

Gaudemer, Y., Tapponnier, P., Meyer, B., Peltzer, G., Shunmin, G., and Zhitai, C., et al., 1995, Partitioning of crustal slip between linked, active faults in the eastern Qilian Shan, and evidence for a major seismic gap, the "Tianzhu gap," on the western Haiyuan fault, Gansu (China): Geophysical Journal International, v. 120, no. 3, p. 599–645, https://doi.org/10.1111/j.1365-246X.1995.tb01842.x.

George, A.D., Marshallsea, S.J., Wyrwoll, K.H., Chen, J., and Lu, Y., 2001, Miocene cooling in the northern Qilian Shan, northeastern margin of the Tibetan Plateau, revealed by apatite fission-track and vitrinite-reflectance analysis: Geology, v. 29, no. 10, p. 939–942, https://doi.org/10.1130/0091-7613(2001)029<0939:MCITNQ>2.0.CO;2.

Gleadow, A.J.W., and Duddy, I.R., 1981, A natural long-term track annealing experiment for apatite: Nuclear Tracks, v. 5, no. 1–2, p. 169–174, https://doi.org/10.1016/0191-278X(81)90039-1.

Gleadow, A.J., Kohn, B.P., Brown, R.W., O'Sullivan, P.B., and Raza, A., 2002, Fission track thermotectonic imaging of the Australian continent: Tectonophysics, v. 349, no. 1–4, p. 5–21, https://doi.org/10.1016/S0040-1951(02)00043-4.

Gleadow, A.J.W., 1981, Fission-track dating methods: What are the real alternatives?: Nuclear Tracks, v. 5, p. 3–14, https://doi.org/10.1016/0191-278X(81)90021-4.

Gleadow, A.J.W., Duddy, I.R., Green, P.F., and Lovering, J.F., 1986, Confined fission track lengths in apatite: A diagnostic tool for thermal history analysis: Contributions to Mineralogy and Petrology, v. 94, p. 405–415, https://doi.org/10.1007/BF00376334.

Gong, J.H., Zhang, J.X., and Yu, S.Y., 2013, Redefinition of the Longshoushan Group outcropped in the eastern segment of Longshoushan on the southern margin of Alxa Block: Evidence from detrital zircon U-Pb dating results [in Chinese with English Abstract]: Acta Petrologica et Mineralogica, v. 32, no. 1, p. 1–22.

Gong, J.H., Zhang, J.X., Wang, Z.Q., Yu, S.Y., Li, H.K., and Li, Y.S., 2016, Origin of the Alxa Block, western China: New evidence from zircon U-Pb geochronology and Hf isotopes of the Longshoushan Complex: Gondwana Research, v. 36, p. 359–375, https://doi.org/10.1016/j.gr.2015.06.014.

Green, P.F., 1988, The relationship between track shortening and fission track age reduction in apatite: Combined influences of inherent instability, annealing anisotropy, length bias and system calibration: Earth and Planetary Science Letters, v. 89, no. 3–4, p. 335–352, https://doi.org/10.1016/0012-821X(88)90121-5.

Green, P.F., Duddy, I.R., Gleadow, A.J.W., Laslett, G.M., and Tingate, P.R., 1986, Thermal annealing of fission track in apatite 1: A qualitative description: Chemical Geology, v. 59, p. 237–253, https://doi.org/10.1016/0168-9622(86)90074-6.

Guo, X.Y., Gao, R., Li, S.Z., Xu, X., Huang, X.F., Wang, H.Y., Li, W.H., Zhao, S.J., and Li, X.Y., 2016, Lithospheric architecture and deformation of NE Tibet: New insights on the interplay of regional tectonic processes: Earth and Planetary Science Letters, v. 449, p. 89–95, https://doi.org/10.1016/j.epsl.2016.05.045.

He, P., Wang, X., Song, C., Wang, Q., Deng, L., and Zhong, S., 2017, Cenozoic evolution of the Western Qinling Mt. Range based on thermochronologic and sedimentary records from the Wudu Basin, NE Tibetan Plateau: Journal of Asian Earth Sciences, v. 138, p. 484–494, https://doi.org/10.1016/j.jseaes.2017.02.033.

He, P., Song, C., Wang, Y., Meng, Q., Chen, L., Yao, L., Huang, S., Feng, W., and Chen, S., 2018, Cenozoic deformation history of the Qilian Shan (northeastern Tibetan Plateau) constrained by detrital apatite fission-track thermochronology in the northeastern Qaidam Basin: Tectonophysics, v. 749, no. 6, p. 1–11, https://doi.org/10.1016/j.tecto.2018.10.017.

He, P., Song, C., Wang, Y., Meng, Q., Wang, D., Feng, Y., Chen, L., and Feng, W., 2020, Early Cenozoic exhumation in the Qilian Shan, northeastern margin of the Tibetan Plateau: Insights from detrital apatite fission track thermochronology: Terra Nova, v. 32, p. 415–424, https://doi.org/10.1111/ter.12478.

Horton, B.K., Dupont-Nivet, G., Zhou, J., Waanders, G.L., Butler, R.F., and Wang, J., 2004, Mesozoic-Cenozoic evolution of the Xining-Minhe and Dangchang basins, northeastern Tibetan Plateau: Magnetostratigraphic and biostratigraphic results: Journal of Geophysical Research: Solid Earth, v. 109, no. B04402, https://doi.org/10.1029/2003JB002913.

Huo, Y.L., and Tan, S.D., 1995, Exploration Case History and Petroleum Geology in Jiuquan Continental Basin: Beijing, China, Petroleum Industry Press, 211 p.

Hurford, A.J., 1990, Standardization of fission track dating calibration: Recommendation by the Fission Track Working Group of the IUGS Subcommission on Geochronology: Chemical Geology: Isotope Geoscience Section, v. 80, p. 171–178, https://doi.org/10.1016/0168-9622(90)90025-8.

Hurford, A.J., and Green, P.F., 1983, The zeta age calibration of fission-track dating: Chemical Geology, v. 41, p. 285–317, https://doi.org/10.1016/S0009-2541(83)80026-6.

Ji, J., Zhang, K., Clift, P.D., Zhuang, G., Song, B., and Ke, X., 2017, High-resolution magnetostratigraphic study of the Paleogene-Neogene strata in the northern Qaidam basin: implications for the growth of the northeastern Tibetan plateau: Gondwana Research, v. 46, p. 141–155, https://doi.org/10.1016/j.gr.2017.02.015.

Jolivet, M., Brunel, M., Seward, D., Xu, Z., Yang, J., Roger, F., and Wu, C., 2001, Mesozoic and Cenozoic tectonics of the northern edge of the Tibetan Plateau: Fission-track constraints: Tectonophysics, v. 343, no. 1–2, p. 111–134, https://doi.org/10.1016/S0040-1951(01)00196-2.

Jolivet, M., Roger, F., Xu, Z.Q., Paquette, J.L., and Cao, H., 2015, Mesozoic–Cenozoic evolution of the Danba dome (Songpan Garzê, East Tibet) as inferred from LA-ICP-MS U–Pb and fission-track data: Journal of Asian Earth Sciences, v. 102, p. 180–204, https://doi.org/10.1016/j.jseaes.2015.02.009.

Kapp, P., and DeCelles, P.G., 2019, Mesozoic-Cenozoic geological evolution of the Himalayan-Tibetan orogen and working tectonic hypotheses: American Journal of Science, v. 319, p. 159–254, https://doi.org/10.2475/03.2019.01.

Kapp, P., DeCelles, P.G., Gehrels, G.E., Heizler, M., and Ding, L., 2007, Geological records of the Lhasa-Qiangtang and Indo-Asian collisions in the Nima area of central Tibet: Geological Society of America Bulletin, v. 119, no. 7–8, p. 917–933, https://doi.org/10.1130/B26033.1.

Kaya, M.Y., Dupont-Nivet, G., Proust, J.N., Roperch, P., Bougeois, L., Meijer, N., and Barbolini, N., 2019, Paleogene evolution and demise of the proto-Paratethys Sea in Central Asia (Tarim and Tajik basins): Role of intensified tectonic activity at ca. 41 Ma: Basin Research, v. 31, no. 3, p. 461–486, https://doi.org/10.1111/bre.12330.

Ketcham, R.A., 2005, Forward and inverse modeling of low-temperature thermochronometry data: Reviews in Mineralogy and Geochemistry, v. 58, p. 275–314, https://doi.org/10.2138/rmg.2005.58.11.

Ketcham, R.A., Carter, A., Donelick, R.A., Barbarand, J., and Hurford, A.J., 2007, Improved modeling of fission-track annealing in apatite: The American Mineralogist, v. 92, no. 5–6, p. 799–810, https://doi.org/10.2138/am.2007.2281.

Ketcham, R.A., Donelick, R.A., Balestrieri, M.L., and Zattin, M., 2009, Reproducibility of apatite fission-track length data and thermal history reconstruction: Earth and Planetary Science Letters, v. 284, no. 3–4, p. 504–515, https://doi.org/10.1016/j.epsl.2009.05.015.

Laslett, G.M., Green, P.F., Duddy, I.R., and Gleadow, A.J.W., 1987, Thermal annealing of fission tracks in apatite; 2: A quantitative analysis: Chemical Geology. Isotope Geoscience Section, v. 65, p. 1–13, https://doi.org/10.1016/0168-9622(87)90057-1.

Lease, R.O., Burbank, D.W., Clark, M.K., Farley, K.A., Zheng, D., and Zhang, H., 2011, Middle Miocene reorganization of deformation along the northeastern Tibetan Plateau: Geology, v. 39, no. 4, p. 359–362, https://doi.org/10.1130/G31356.1.

Lease, R.O., Burbank, D.W., Hough, B., Wang, Z., and Yuan, D., 2012, Pulsed Miocene range growth in northeastern Tibet: Insights from Xunhua Basin magnetostratigraphy and provenance: Geological Society of America Bulletin, v. 124, no. 5–6, p. 657–677, https://doi.org/10.1130/B30524.1.

Li, B., Yan, M., Zhang, W., Fang, X., Meng, Q., Zan, J., Chen, Y., Zhang, D., Yang, Y., and Guan, Y., 2017a, New paleomagnetic constraints on middle Miocene strike-slip faulting along the middle Altyn Tagh Fault: Journal of Geophysical Research: Solid Earth, v. 122, p. 4106–4122, https://doi.org/10.1002/2017JB014058.

Li, B., Chen, X., Zuza, A.V., Hu, D., Ding, W., Huang, P., and Xu, S., 2019, Cenozoic cooling history of the North Qilian Shan, northern Tibetan Plateau, and the initiation of the Haiyuan fault: Constraints from apatite-and zircon-fission track thermochronology: Tectonophysics, v. 751, p. 109–124, https://doi.org/10.1016/j.tecto.2018.12.005.

Li, B., Zuza, A.V., Chen, X., Hu, D., Shao, Z., Qi, B., Wang, Z., Levy, D.A., and Xiong, X., 2020, Cenozoic multiphase deformation in the Qilian Shan and out-of-sequence development of the northern Tibetan Plateau: Tectonophysics, v. 782–783, no. 228423, https://doi.org/10.1016/j.tecto.2020.228423.

Li, H.S., Wu, C., Luo, T.W., Jiang, T., Chen, Y.F., and Wang, G.H., 2017b, Ages and geochemistry of the Renacuo granitoids in the Gaize area, central Tibet: Implications for the northward subduction of the Bangong Suture Ocean: Geological Journal, v. 52, p. 14–29, https://doi.org/10.1002/gj.2717.

Lin, X., Chen, H., Wyrwoll, K.H., Batt, G.E., Liao, L., and Xiao, J., 2011, The uplift history of the Haiyuan-Liupan Shan region northeast of the present Tibetan Plateau: Integrated constraint from stratigraphy and thermochronology: The Journal of Geology, v. 119, no. 4, p. 372–393, https://doi.org/10.1086/660190.

Lin, X., Zheng, D., Sun, J., Windley, B.F., Tian, Z., Gong, Z., and Jia, Y., 2015, Detrital apatite fission track evidence for provenance change in the Subei Basin and implications for the tectonic uplift of the Danghenan Shan (NW China) since the mid-Miocene: Journal of Asian Earth Sciences, v. 111, p. 302–311, https://doi.org/10.1016/j.jseaes.2015.07.007.

Liu, C.C., Wang, W.T., Zhang, P.Z., Pang, J.Z., and Yu, J.X., 2016, Magnetostratigraphy and magnetic anisotropy of the Neogene sediments in the Qilian Basin [in Chinese with English Abstract]: Chinese Journal of Geophysics, v. 59, no. 8, p. 2965–2978.

Liu, D., Li, H., Sun, Z., Pan, J., Wang, M., and Wang, H., 2017a, AFT dating constrains the Cenozoic uplift of the Qimen Tagh Mountains, Northeast Tibetan Plateau, comparison with LA-ICPMS Zircon U–Pb ages: Gondwana Research, v. 41, p. 438–450, https://doi.org/10.1016/j.gr.2015.10.008.

Liu, H.B., Kong, X.X., Ma, X.B., Wang, Q.S., Yan, Y.L., Yan, Y.F., and Yang, Z.Q., 2001, Physical structure features of the crust at southeast region of Tibetan Plateau [series D]: Science in China, v. 44, p. 64–71, https://doi.org/10.1007/BF02911972.

Liu, R., Allen, M.B., Zhang, Q., Du, W., Cheng, X., Holdsworth, R.E., and Guo, Z., 2017b, Basement controls on deformation during oblique convergence: Transpressive structures in the western Qaidam Basin, northern Tibetan Plateau: Lithosphere, v. 9, p. 583–594, https://doi.org/10.1130/L634.1.

Meyer, B., Tapponnier, P., Bourjot, L., Metivier, F., Gaudemer, Y., and Peltzer, G., et al., 1998, Crustal thickening in Gansu-Qinghai, lithospheric mantle subduction, and oblique, strike-slip controlled growth of the Tibet plateau: Geophysical Journal International, v. 135, p. 1–47, https://doi.org/10.1046/j.1365-246X.1998.00567.x.

Mock, C., Arnaud, N.O., and Cantagrel, J.M., 1999, An early unroofing in northeastern Tibet? Constraints from $^{40}Ar/^{39}Ar$ thermochronology on granitoids from the Eastern Kunlun Range (Qianghai, NW China): Earth and Planetary Science Letters, v. 171, p. 107–122, https://doi.org/10.1016/S0012-821X(99)00133-8.

Palumbo, L., Hetzel, R., Tao, M., and Li, X., 2010, Topographic and lithologic control on catchment-wide denudation rates derived from cosmogenic ^{10}Be in two mountain ranges at the margin of NE Tibet: Geomorphology, v. 117, p. 130–142, https://doi.org/10.1016/j.geomorph.2009.11.019.

Pan, G.T., Ding, J., Yao, D., and Wang, L., 2004, Geological map of Qinghai-Xiang (Tibet) plateau and adjacent areas: Chengdu Institute of Geology and Mineral Resources, China Geological Survey, scale 1:1,500,000.

Pang, J., Yu, J., Zheng, D., Wang, W., Ma, Y., Wang, Y., et al., 2019, Neogene expansion of the Qilian Shan, north Tibet: Implications for the dynamic evolution of the Tibetan Plateau: Tectonics, v. 38, p. 1018–1032, https://doi.org/10.1029/2018TC005258.

Pullen, A., Kapp, P., Gehrels, G.E., Vervoort, J.D., and Ding, L., 2008, Triassic continental subduction in central Tibet and Mediterranean-style closure of the Paleo-Tethys Ocean: Geology, v. 36, no. 5, p. 351–354, https://doi.org/10.1130/G24435A.1.

Qi, B., Hu, D., Yang, X., Zhang, Y., Tan, C., Zhang, P., and Feng, C., 2016, Apatite fission track evidence for the Cretaceous-Cenozoic cooling history of the Qilian Shan (NW China) and for stepwise northeastward growth of the northeastern Tibetan Plateau since early Eocene: Journal of Asian Earth Sciences, v. 124, p. 28–41, https://doi.org/10.1016/j.jseaes.2016.04.009.

Qinghai, B.G.M.R. (Bureau of Geology and Mineral Resources), 1991, Regional Geology of Qinghai Province [in Chinese with English summary]: Geological Publishing House, Beijing, 662 p.

Ren, J.S., Niu, B.G., Wang, J., Jin, X.C., and Xie, L.Z., 2013, 1:5 Million international geological map of Asia: Acta Geoscientica Sinica, v. 34, no. 1, p. 24–24.

Ritts, B.D., Yue, Y., Graham, S.A., Sobel, E.R., Abbink, O.A., and Stockli, D., 2008, From sea level to high elevation in 15 million years: Uplift history of the northern Tibetan Plateau margin in the Altun Shan: American Journal of Science, v. 308, no. 5, p. 657–678, https://doi.org/10.2475/05.2008.01.

Royden, L.H., Burchfiel, B.C., and van der Hilst, R.D., 2008, The geological evolution of the Tibetan Plateau: Science, v. 321, p. 1054–1058, https://doi.org/10.1126/science.1155371.

Ryan, W.B.F., Carbotte, S.M., Coplan, J.O., O'Hara, S., Melkonian, A., Arko, R., Weissel, R.A., Ferrini, V., Goodwillie, A., Nitsche, F., Bonczkowski, J., and Zemsky, R., 2009, Global multiresolution topography synthesis: Geochemistry Geophysics Geosystems, v. 10, p. Q03014, https://doi.org/10.1029/2008GC002332.

Shi, W., Wang, F., Yang, L., Wu, L., and Zhang, W., 2018, Diachronous growth of the Altyn Tagh Mountains: Constraints on propagation of the northern Tibetan margin from (U-Th)/He dating: Journal of Geophysical Research: Solid Earth, v. 123, p. 6000–6018, https://doi.org/10.1029/2017JB014844.

Sobel, E.R., Chen, J., and Heermance, R.V., 2006a, Late Oligocene early Miocene initiation of shortening in the Southwestern Chinese Tian Shan: Implications for Neogene shortening rate variations: Earth and Planetary Science Letters, v. 247, p. 70–81, https://doi.org/10.1016/j.epsl.2006.03.048.

Sobel, E.R., Oskin, M., Burbank, D., and Miskolaichuk, A., 2006b, Exhumation of basement-cored uplifts: example of the Kyrgyz range quantified with apatite fission track thermochronology: Tectonics, v. 25, no. 2, https://doi.org/10.1029/2005TC001809.

Song, D., Glorie, S., Xiao, W., Collins, A., Gillespie, J., Jepson, G., and Li, Y., 2018, Tectono-thermal evolution of the southwestern Alxa Tectonic Belt, NW China: Constrained by apatite U-Pb and fission track thermochronology: Tectonophysics, v. 722, p. 577–594, https://doi.org/10.1016/j.tecto.2017.11.029.

Song, S.G., Niu, Y., Su, L., and Xia, X., 2013, Tectonics of the North Qilian orogen, NW China: Gondwana Research, v. 23, no. 4, p. 1378–1401, https://doi.org/10.1016/j.gr.2012.02.004.

Staisch, L.M., Niemi, N.A., Clark, M.K., and Chang, H., 2016, Eocene to late Oligocene history of crustal shortening within the Hoh Xil Basin and implications for the uplift history of the northern Tibetan Plateau: Tectonics, v. 35, no. 4, p. 862–895, https://doi.org/10.1002/2015TC003972.

Sun, J., Zhu, R., and An, Z., 2005, Tectonic uplift in the northern Tibetan Plateau since 13.7 Ma ago inferred from molasse deposits along the Altyn Tagh Fault: Earth and Planetary Science Letters, v. 235, no. 3–4, p. 641–653, https://doi.org/10.1016/j.epsl.2005.04.034.

Tang, Z.L., and Bai, Y.L., 2000, The geotectonic setting of the large and superlange mineral deposits in the southwest margin of North China Paleoplate [in Chinese with English Abstract]: Acta Geologica Gansu. v. 9, no. 1, p. 1–14.

Tapponnier, P., Zhiqin, X., Roger, F., Meyer, B., Arnaud, N., Wittlinger, G., and Jingsui, Y., 2001, Oblique stepwise rise and growth of the Tibet Plateau: Science, v. 294, no. 5547, p. 1671–1677, https://doi.org/10.1126/science.105978.

Taylor, M., and Yin, A., 2009, Active structures of the Himalayan-Tibetan orogen and their relationships to earthquake distribution, contemporary strain field, and Cenozoic volcanism: Geosphere, v. 5, no. 3, p. 199–214, https://doi.org/10.1130/GES00217.1.

Taylor, M., Yin, A., Ryerson, F.J., Kapp, P., and Ding, L., 2003, Conjugate strike-slip faulting along the Bangong-Nujiang suture zone accommodates coeval east-west extension and north-south shortening in the interior of the Tibetan Plateau: Tectonics, v. 22, https://doi.org/10.1029/2002TC001361.

Tian, P., Yuan, W., Yang, X., Feng, Z., Chen, X., and Yuan, E., 2020, Multi-stage tectonic events of the Eastern Kunlun Mountains, Northern Tibetan Plateau constrained by fission track thermochronology: Journal of Asian Earth Sciences, v. 198, no. 104428, https://doi.org/10.1016/j.jseaes.2020.104428.

van der Beek, P., Robert, X., Mugnier, J.L., Bernet, M., Huyghe, P., and Labrin, E., 2006, Late Miocene–recent exhumation of the central Himalaya and recycling in the foreland basin assessed by apatite fission-track thermochronology of Siwalik sediments, Nepal: Basin Research, v. 18, no. 4, p. 413–434, https://doi.org/10.1111/j.1365-2117.2006.00305.x.

Van der Voo, R., van Hinsbergen, D.J., Domeier, M., Spakman, W., and Torsvik, T.H., 2015, Latest Jurassic–earliest Cretaceous closure of the Mongol-Okhotsk Ocean: A paleomagnetic and seismological-tomographic analysis, *in* Anderson, T.H., Didenko, A.N., Johnson, C.L., Khanchuk, A.I., and MacDonald, Jr., J.H., eds., Late Jurassic Margin of Laurasia–A Record of Faulting Accommodating Plate Rotation: Geological Society of America Special Paper 513, p. 589–606, https://doi.org/10.1130/2015.2513(19).

Vermeesch, P., 2009, RadialPlotter: a Java application for fission track, luminescence and other radial plots: Radiation Measurements, v. 44, p. 409–410, https://doi.org/10.1016/j.radmeas.2009.05.003.

Vermeesch, P., 2012, On the visualisation of detrital age distributions: Chemical Geology, v. 312, p. 190–194, https://doi.org/10.1016/j.chemgeo.2012.04.021.

Vincent, S.J., and Allen, M.B., 1999, Evolution of the Minle and Chaoshui Basins, China: Implications for Mesozoic strike-slip basin formation in Central Asia: Geological Society of America Bulletin, v. 111, no. 5, p. 725–742, https://doi.org/10.1130/0016-7606(1999)111<0725:EOTMAC>2.3.CO;2.

Wang, C.S., Dai, J.G., Zhao, X.X., Li, Y.L., Graham, S.A., He, D.F., Ran, B., and Meng, J., 2014, Outward-growth of the Tibetan Plateau during the Cenozoic: A review: Tectonophysics, v. 621, p. 1–43, https://doi.org/10.1016/j.tecto.2014.01.036.

Wang, E., and Burchfiel, B.C., 2004, Late Cenozoic right-lateral movement along the Wenquan fault and associated deformation: Implications for the kinematic history of the Qaidam Basin, northeastern Tibetan Plateau: International Geology Review, v. 46, no. 10, p. 861–879, https://doi.org/10.2747/0020-6814.46.10.861.

Wang, F., Shi, W., Zhang, W., Wu, L., Yang, L., Wang, Y., and Zhu, R., 2017a, Differential growth of the northern Tibetan margin: Evidence for oblique stepwise rise of the Tibetan Plateau: Scientific Reports, v. 7, no. 41164, https://doi.org/10.1038/srep41164.

Wang, W., Zheng, W., Zhang, P., Li, Q., Kirby, E., and Yuan, D., et al., 2017b, Expansion of the Tibetan Plateau during the Neogene: Nature Communications, v. 8, no. 1, p. 15,887, https://doi.org/10.1038/ncomms15887.

Wang, W., Zheng, D., Li, C., Wang, Y., Zhang, Z., Pang, J., Wang, Y., Yu, J., Wang, Y., Zheng, W., Zhang, H., and Zhang, P., 2020a, Cenozoic exhumation of the Qilian Shan in the northeastern Tibetan Plateau: Evidence from low-temperature thermochronology: Tectonics, v. 39, no. e2019TC005705, https://doi.org/10.1029/2019TC005705.

Wang, W.T., Zhang, P.Z., Kirby, E., Wang, L.H., Zhang, G.L., Zheng, D.W., and Chai, C.Z., 2011, A revised chronology for Tertiary sedimentation in the Sikouzi basin: Implications for the tectonic evolution of the northeastern corner of the Tibetan Plateau: Tectonophysics, v. 505, no. 1–4, p. 100–114, https://doi.org/10.1016/j.tecto.2011.04.006.

Wang, X., Wang, B., Qiu, Z., Xie, G., Xie, J., and Downs, W., et al., 2003, Danghe area (western Gansu, China) biostratigraphy and implications for depositional history and tectonics of northern Tibetan Plateau: Earth and Planetary Science Letters, v. 208, no. 3–4, p. 253–269, https://doi.org/10.1016/S0012-821X(03)00047-5.

Wang, Y., Zheng, J., and Zheng, Y., 2018, Mesozoic-Cenozoic exhumation history of the Qimen Tagh Range, northeastern margins of the Tibetan Plateau: Evidence from apatite fission track analysis: Gondwana Research, v. 58, p. 16–26, https://doi.org/10.1016/j.gr.2018.01.014.

Wang, Z.Z., Chen, X.H., Shao, Z.G., Li, B., Ding, W.C., Zhang, Y.P., Wang, Y.C., Xu, S.L., and Qin, X., 2020b, Petrogenesis of the Late Silurian-early Devonian granites in the Longshoushan-Helishan area, Gansu Province, and its tectonic implications for the Early Paleozoic evolution of the southwestern Alxa Block [in Chinese with English Abstract]: Acta Geologica Sinica, v. 94, no. 8, p. 2243–2261.

Wu, C., Yin, A., Zuza, A.V., Zhang, J., Liu, W., and Ding, L., 2016, Pre-Cenozoic geologic history of the central and northern Tibetan Plateau and the role of Wilson cycles in constructing the Tethyan orogenic system: Lithosphere, v. 8, no. 3, p. 254–292, https://doi.org/10.1130/L494.1.

Wu, C., Zuza, A.V., Yin, A., Liu, C., Reith, R.C., Zhang, J., Liu, W.C., and Zhou, Z., 2017, Geochronology and geochemistry of Neoproterozoic granitoids in the central Qilian Shan of northern Tibet: Reconstructing the amalgamation processes and tectonic history of Asia: Lithosphere, v. 9, p. 609–636, https://doi.org/10.1130/L640.1.

Wu, C., Zuza, A.V., Chen, X., Ding, L., Levy, D.A., Liu, C., Liu, W., Jiang, T., and Stockli, D.F., 2019a, Tectonics of the Eastern Kunlun Range: Cenozoic reactivation of a Paleozoic-Early Mesozoic orogen: Tectonics, v. 38, p. 1609–1650, https://doi.org/10.1029/2018TC005370.

Wu, C., Zuza, A.V., Zhou, Z.G., Yin, A., McRivette, M.W., Chen, X.H., Ding, L., and Geng, J.Z., 2019b, Mesozoic-Cenozoic evolution of the Eastern Kunlun Range, central Tibet, and implications for basin evolution during the Indo-Asian collision: Lithosphere, v. 11, no. 4, p. 524–550, https://doi.org/10.1130/L1065.1.

Wu, C., Liu, C., Fan, S., Zuza, A.V., Ding, L., Liu, W., Ye, B., Yang, S., and Zhou, Z., 2020, Structural analysis and tectonic evolution of the western domain of the Eastern Kunlun Range, northwest Tibet: Geological Society of America Bulletin, v. 132, no. 5–6, p. 1291–1315, https://doi.org/10.1130/B35388.1.

Wu, L., Xiao, A., Wang, L., Shen, Z., Zhou, S., Chen, Y., and Guan, J., 2011, Late Jurassic-early Cretaceous

northern Qaidam basin, NW China: implications for the earliest Cretaceous intracontinental tectonism: Cretaceous Research, v. 32, no. 4, p. 552–564, https://doi.org/10.1016/j.cretres.2011.04.002.

Yan, M., Van der Voo, R., Fang, X., Parés, J.M., and Rea, D.K., 2006, Paleomagnetic evidence for a mid-Miocene clockwise rotation of about 25° of the Guide Basin area in NE Tibet: Earth and Planetary Science Letters, v. 241, no. 1–2, p. 234–247, https://doi.org/10.1016/j.epsl.2005.10.013.

Yang, H., Yang, X., Zhang, H., Huang, X., Huang, W., and Zhang, N., 2018, Active fold deformation and crustal shortening rates of the Qilian Shan foreland thrust belt, NE Tibet, since the late Pleistocene: Tectonophysics, v. 742–743, p. 84–100, https://doi.org/10.1016/j.tecto.2018.05.019.

Yin, A., 2010, Cenozoic tectonic evolution of Asia: A preliminary synthesis: Tectonophysics, v. 488, no. 1–4, p. 293–325, https://doi.org/10.1016/j.tecto.2009.06.002.

Yin, A., and Harrison, T.M., 2000, Geologic Evolution of the Himalayan-Tibetan Orogen: Annual Review of Earth and Planetary Sciences, v. 28, p. 211–280, https://doi.org/10.1146/annurev.earth.28.1.211.

Yin, A., Rumelhart, P.E., Butler, R., Cowgill, E., Harrison, T.M., Foster, D.A., Ingersoll, R.V., Qing, Z., Xian-Qiang, Z., Xiao-Feng, W., Hanson, A., and Raza, A., 2002, Tectonic history of the Altyn Tagh fault system in northern Tibet inferred from Cenozoic sedimentation: Geological Society of America Bulletin, v. 114, no. 10, p. 1257–1295, https://doi.org/10.1130/0016-7606(2002)114<1257:THOTAT>2.0.CO;2.

Yin, A., Dang, Y., Zhang, M., McRivette, M.W., Burgess, W.P., and Chen, X., 2007a, Cenozoic tectonic evolution of Qaidam basin and its surrounding regions (part 2): Wedge tectonics in southern Qaidam basin and the Eastern Kunlun Range, *in* Sears, J.W., Harms, T.A., and Evenchick, C.A., eds., Whence the Mountains? Inquiries into the Evolution of Orogenic Systems: A Volume in Honor of Raymond A. Price: Geological Society of America Special Paper 433, 369–390, https://doi.org/10.1130/2007.2433(18).

Yin, A., Manning, C.E., Lovera, O., Menold, C.A., Chen, X., and Gehrels, G.E., 2007b, Early Paleozoic tectonic and thermomechanical evolution of ultrahigh-pressure (UHP) metamorphic rocks in the northern Tibetan Plateau, Northwest China: International Geology Review, v. 49, no. 8, p. 681–716, https://doi.org/10.2747/0020-6814.49.8.681.

Yin, A., Dang, Y.-Q., Wang, L.-C., Jiang, W.-M., Zhou, S.-P., Chen, X.-H., Gehrels, G.E., and Mcrivette, M.W., 2008a, Cenozoic tectonic evolution of Qaidam basin and its surrounding regions (Part 1): The southern Qilian Shan-Nan Shan thrust belt and northern Qaidam basin: Geological Society of America Bulletin, v. 120, no. 7–8, p. 813–846, https://doi.org/10.1130/B26180.1.

Yin, A., Dang, Y.Q., Zhang, M., Chen, X.H., and McRivette, M.W., 2008b, Cenozoic tectonic evolution of the Qaidam basin and its surrounding regions (Part 3): Structural geology, sedimentation, and regional tectonic reconstruction: Geological Society of America Bulletin, v. 120, no. 7–8, p. 847–876, https://doi.org/10.1130/B26232.1.

Yu, J., Zheng, D., Pang, J., Wang, Y., Fox, M., Vermeesch, P., et al., 2019a, Miocene range growth along the Altyn Tagh fault: Insights from apatite fission track and (U-Th)/He thermochronometry in the western Danghenan Shan, China: Journal of Geophysical Research: Solid Earth, v. 124, p. 9433–9453, https://doi.org/10.1029/2019JB017570.

Yu, J.X., Pang, J.Z., Wang, Y.Z., Zheng, D.W., Liu, C.C., and Wang, W.T., et al., 2019b, Mid-Miocene uplift of the northern Qilian Shan as a result of the northward growth of the northern Tibetan Plateau: Geosphere, v. 15, no. 2, p. 423–432, https://doi.org/10.1130/GES01520.1.

Yu, X.J., Guo, Z., Zhang, Q., Cheng, X., Du, W., Wang, Z., and Bian, Q., 2017, Denan Depression controlled by northeast-directed Olongbulak thrust zone in northeastern Qaidam Basin: Implications for growth of northern Tibetan Plateau: Tectonophysics, v. 717, p. 116–126, https://doi.org/10.1016/j.tecto.2017.06.017.

Yuan, D.Y., Champagnac, J.D., Ge, W.P., Molnar, P., Zhang, P.Z., and Zheng, W.J., et al., 2011, Late Quaternary right-lateral slip rates of faults adjacent to the lake Qinghai, northeastern margin of the Tibetan Plateau: Geological Society of America Bulletin, v. 123, no. 9–10, p. 2016–2030, https://doi.org/10.1130/B30315.1.

Yuan, D.Y., Ge, W.P., Chen, Z.W., Li, C.Y., Wang, Z.C., and Roe, G.H., 2013, The growth of northeastern Tibet and its relevance to large-scale continental geodynamics: A review of recent studies: Tectonics, v. 32, p. 1358–1370, https://doi.org/10.1002/tect.20081.

Yuan, W., Dong, J., Carter, A., Bao, Z., and An, Y., 2006a, Mesozoic-Tertiary exhumation history of the Altai Mountains, northern Xinjiang, China: Constraints from apatite fission track data: Tectonophysics, v. 412, no. 3–4, p. 183–193, https://doi.org/10.1016/j.tecto.2005.09.007.

Yuan, W., Dong, J., Shicheng, W., and Carter, A., 2006b, Apatite fission track evidence for Neogene uplift in the eastern Kunlun Mountains, northern Qinghai–Tibet Plateau, China: Journal of Asian Earth Sciences, v. 27, no. 6, p. 847–856, https://doi.org/10.1016/j.jseaes.2005.09.002.

Zhang, B.H., Zhang, J., Wang, Y.N., Zhao, H., and Li, Y.F., 2017, Late Mesozoic-Cenozoic exhumation of the Northern Hexi Corridor: constrained by apatite fission track ages of the Longshoushan: Acta Geologica Sinica, v. 91, no. 5, p. 1624–1643, https://doi.org/10.1111/1755-6724.13402.

Zhang, C.L., Ye, X.T., Zou, H.B., and Chen, X.Y., 2016, Neoproterozoic sedimentary basin evolution in southwestern Tarim, NW China: New evidence from field observations, detrital zircon U-Pb ages and Hf isotope compositions: Precambrian Research, v. 280, p. 31–45, https://doi.org/10.1016/j.precamres.2016.04.011.

Zhang, J., Wang, Y., Zhang, B., and Zhao, H., 2015, Evolution of the NE Qinghai–Tibetan Plateau, constrained by the apatite fission track ages of the mountain ranges around the Xining Basin in NW China: Journal of Asian Earth Sciences, v. 97, p. 10–23, https://doi.org/10.1016/j.jseaes.2014.10.002.

Zhang, L.Y., Ding, L., Pullen, A., Xu, Q., Liu, D.L., Cai, F.L., Yue, Y.H., Lai, Q.Z., Shi, R.D., Ducea, M.H., Kapp, P., and Chapman, A., 2014, Age and geochemistry of western Hoh-Xil–Songpan-Ganzi granitoids, northern Tibet: Implications for the Mesozoic closure of the Paleo-Tethys ocean: Lithos, v. 190, p. 328–348, https://doi.org/10.1016/j.lithos.2013.12.019.

Zhang, P., Burchfiel, B.C., Molnar, P., Zhang, W., Jiao, D., Deng, Q., Wang, Y., Royden, L., and Song, F., 1991, Amount and style of late Cenozoic deformation in the Liupan Shan area, Ningxia Autonomous Region, China: Tectonics, v. 10, no. 6, p. 1111–1129, https://doi.org/10.1029/90TC02686.

Zhang, P.Z., Shen, Z., Wang, M., Gan, W., Bürgmann, R., Molnar, P., and Hanrong, S., 2004, Continuous deformation of the Tibetan Plateau from global positioning system data: Geology, v. 32, no. 9, p. 809–812, https://doi.org/10.1130/G20554.1.

Zheng, D., Zhang, P.Z., Wan, J., Yuan, D., Li, C., and Yin, G., et al., 2006, Rapid exhumation at ~8 Ma on the Liupan Shan thrust fault from apatite fission-track thermochronology: Implications for growth of the northeastern Tibetan Plateau margin: Earth and Planetary Science Letters, v. 248, no. 1–2, p. 198–208, https://doi.org/10.1016/j.epsl.2006.05.023.

Zheng, D., Clark, M.K., Zhang, P., Zheng, W., and Farley, K.A., 2010, Erosion, fault initiation and topographic growth of the North Qilian Shan (northern Tibetan Plateau): Geosphere, v. 6, no. 6, p. 937–941, https://doi.org/10.1130/GES00523.1.

Zheng, D., Wang, W., Wan, J., Yuan, D., Liu, C., Zheng, W., et al., 2017, Progressive northward growth of the northern Qilian Shan-Hexi Corridor (northeastern Tibet) during the Cenozoic: Lithosphere, v. 9, no. 3, p. 408–416, https://doi.org/10.1130/L587.1.

Zheng, W.J., Zhang, P.Z., and Ge, W.P., et al., 2013, Late Quaternary slip rate of the South Heli Shan Fault (northern Hexi Corridor, NW China) and its implications for northeastward growth of the Tibetan Plateau: Tectonics, v. 32, no. 2, p. 271–293, https://doi.org/10.1002/tect.20022.

Zhuang, G., Johnstone, S.A., Hourigan, J., Ritts, B., Robinson, A., and Sobel, E.R., 2018, Understanding the geologic evolution of Northern Tibetan Plateau with multiple thermochronometers: Gondwana Research, v. 58, p. 195–210, https://doi.org/10.1016/j.gr.2018.02.014.

Zuza, A.V., and Yin, A., 2016, Continental deformation accommodated by non-rigid passive bookshelf faulting: An example from the Cenozoic tectonic development of northern Tibet: Tectonophysics, v. 677–678, p. 227–240, https://doi.org/10.1016/j.tecto.2016.04.007.

Zuza, A.V., Cheng, X., and Yin, A., 2016, Testing models of Tibetan Plateau formation with Cenozoic shortening estimates across the Qilian Shan–Nan Shan thrust belt: Geosphere, v. 12, p. 501–532, https://doi.org/10.1130/GES01254.1.

Zuza, A.V., Wu, C., Reith, R.C., Yin, A., Li, J.H., Zhang, J.Y., Zhang, Y.X., Wu, L., and Liu, W.C., 2018, Tectonic evolution of the Qilian Shan: An early Paleozoic orogen reactivated in the Cenozoic: Geological Society of America Bulletin, v. 130, no. 5–6, p. 881–925, https://doi.org/10.1130/B31721.1.

Zuza, A.V., Wu, C., Wang, Z., Levy, D.A., Li, B., Xiong, X., and Chen, X., 2019, Underthrusting and duplexing beneath the northern Tibetan Plateau and the evolution of the Himalayan-Tibetan orogen: Lithosphere, v. 11, no. 2, p. 209–231, https://doi.org/10.1130/L1042.1.

Zuza, A.V., Gavillot, Y., Haproff, P.J., and Wu, C., 2020, Kinematic evolution of a continental collision: Constraining the Himalayan-Tibetan orogen via bulk strain rates: Tectonophysics, v. 797, no. 228642, https://doi.org/10.1016/j.tecto.2020.228642.

Science Editor: Rob Strachan
Associate Editor: Timothy Kusky

Manuscript Received 26 August 2020
Revised Manuscript Received 7 January 2021
Manuscript Accepted 20 January 2021

Printed in the USA